Dynamical mean-field theory of the Anderson-Hubbard model with local and nonlocal disorder in tensor formulation

A. Weh [1,*] Y. Zhang [2] A. Östlin [3,4] H. Terletska [5] D. Bauernfeind [6] K.-M. Tam [7,8] H. G. Evertz [9] K. Byczuk [10] D. Vollhardt [3] and L. Chioncel [3,4]

[1] *Theoretical Physics II, Institute of Physics, University of Augsburg, 86135 Augsburg, Germany*
[2] *Kavli Institute of Theoretical Sciences, University of Chinese Academy of Sciences, Beijing 100190, China*
[3] *Theoretical Physics III, Center for Electronic Correlations and Magnetism, Institute of Physics, University of Augsburg, 86135 Augsburg, Germany*
[4] *Augsburg Center for Innovative Technologies, University of Augsburg, 86135 Augsburg, Germany*
[5] *Department of Physics and Astronomy, Middle Tennessee State University, Murfreesboro, Tennessee 37132, USA*
[6] *Center for Computational Quantum Physics, Flatiron Institute, 162 5th Avenue, New York, New York 10010, USA*
[7] *Department of Physics & Astronomy, Louisiana State University, Baton Rouge, Louisiana 70803, USA*
[8] *Center for Computation & Technology, Louisiana State University, Baton Rouge, Louisiana 70803, USA*
[9] *Institute of Theoretical and Computational Physics, Graz University of Technology, 8010 Graz, Austria*
[10] *Institute of Theoretical Physics, Faculty of Physics, University of Warsaw, ulica Pasteura 5, 02-093 Warszawa, Poland*

(Received 17 May 2021; revised 30 June 2021; accepted 1 July 2021; published 16 July 2021)

To explore correlated electrons in the presence of local and nonlocal disorder, the Blackman-Esterling-Berk method for averaging over off-diagonal disorder is implemented into dynamical mean-field theory using tensor notation. The impurity model combining disorder and correlations is solved using the recently developed fork tensor-product state solver, which allows one to calculate the single particle spectral functions on the real-frequency axis. In the absence of off-diagonal hopping, we establish exact bounds of the spectral function of the noninteracting Bethe lattice with coordination number Z. In the presence of interaction, the Mott insulating paramagnetic phase of the one-band Hubbard model is computed at zero temperature in alloys with site- and off-diagonal disorder. When the Hubbard U parameter is increased, transitions from an alloy band insulator through a correlated metal into a Mott insulating phase are found to take place.

DOI: 10.1103/PhysRevB.104.045127

I. INTRODUCTION

The electronic structure and transport properties of real materials are strongly influenced by the Coulomb interaction between the electrons and the presence of disorder [1–3]. In particular, both electronic correlations and randomness are driving forces behind a transition from a metallic to an insulating state due to the localization of electrons [metal-insulator transition (MIT)]. While the Mott-Hubbard MIT is caused by the repulsive interaction between the electrons [2,4,5], the Anderson MIT is a result of coherent backscattering of noninteracting electrons from randomly distributed impurities [1,6–8]. The interplay between interactions and static disorder gives rise to many unusual and often unexpected phenomena [1,3,8–12]. The simplest model of disordered interacting electrons is the Anderson-Hubbard model, obtained by supplementing a single-band Hubbard model with local and/or nonlocal disorder. If the disorder acts only locally, i.e., via random local potentials ("diagonal disorder"), this model is able to describe substitutionally disordered binary alloys. However, in general disorder also affects the amplitudes for hopping between two sites—especially when the bandwidths of the host and dopant are very different—leading to additional "off-diagonal disorder." In analytic calculations local disorder is easier to treat and was studied extensively [13]. In particular, the coherent potential approximation (CPA) [14–19] provides the best single-site approximation for noninteracting systems with local disorder. For that reason the simultaneous investigation of diagonal disorder within the CPA and of interacting electrons with local (Hubbard) interaction within the dynamical mean-field theory (DMFT) [20–24] fit together particularly well, since both DMFT [20,23] and CPA [25,26] become exact in the limit of infinite spatial dimensions or lattice coordination number.

The treatment of the Anderson-Hubbard model with off-diagonal disorder received somewhat less attention [27–32]. In particular, Dobrosavljević and Kotliar [28,29] investigated this model within DMFT by employing a functional integral representation for quantum averages and the replica method for disorder averaging. Thereby they were able to study Hubbard models with arbitrary disorder on Bethe lattices, as well as models on an arbitrary lattice with a special distribution of the off-diagonal disorder, expressed by random hopping amplitudes. In this way they studied the formation of local moments and the Mott transition in disordered systems.

Off-diagonal disorder can also be due to the environment of a local disorder potential. In 1971 Blackman, Esterling,

*andreas.weh@physik.uni-augsburg.de

 ©2021 American Physical Society

and Berk (BEB) [33,34] showed that this type of off-diagonal disorder can, in principle, be incorporated into the CPA framework, such that both diagonal and off-diagonal disorder are tractable within a single-site approximation. In the absence of electronic interactions the BEB formalism was incorporated into the dynamical cluster approximation within the typical medium cluster theory [35] and applied to multiband systems [36].

In our paper we extend these investigations of disordered systems by including a local ("Hubbard") interaction between the electrons. To this end we investigate the Anderson-Hubbard model with diagonal and off-diagonal disorder within the CPA in the BEB formulation [33,34] in a tensor formulation [37,38], while correlation effects are treated within the DMFT [23]. We compute the spectral function and discuss the occurrence of the MIT in the presence of diagonal and off-diagonal disorder. For these purposes an accurate zero-temperature many-body solver on the real energies is used, the so-called fork tensor-product state solver [39]. We observe successive alloy-insulator-to-metal and metal-to-Mott-insulator transitions with increasing values of the Hubbard U parameter. A similar transition scenario was previously discussed for models with diagonal disorder solved within DMFT, but using finite temperature solvers such as the Hirsch-Fye algorithm [40] or the perturbative noncrossing approximation [41]. Contrary to the diagonal disorder model in which the CPA solution provides a common bandwidth for all alloy components, the presence of off-diagonal elements causes the formation of different effective bandwidths for alloy components.

The paper is organized as follows. In Sec. II the BEB theory of the multicomponent Anderson-Hubbard model is formulated, and the computational scheme is discussed. In Sec. III numerical results for a single-band Bethe lattice are presented. Comparison with earlier results on DMFT+CPA allow us to identify effects specifically due to off-diagonal disorder. Finally, conclusions and a summarizing discussion are presented in Sec. IV.

II. BLACKMAN-ESTERLING-BERK THEORY FOR THE ANDERSON-HUBBARD MODEL

In the simplest case an alloy consists of two types of atoms, A and B, with diagonal substitutional disorder, such that only the site-diagonal elements of the Hamiltonian vary stochastically according to the atomic species occupying the given site [14–16]. The physical quantities of interest, for instance the spectral function, are those averaged over the possible disorder realizations. Therefore, the idea of the CPA is to replace the ensemble with random configurations by a periodic system with "average" atoms, whose properties are determined self-consistently. The CPA finds a natural description in the language of scattering theory. Assuming the origin to be occupied by atoms of type A or B and all other sites by average atoms, the scattering by the atom at the origin is easily computed. The self-consistency condition of the CPA, which expresses that the scattering at the origin vanishes on average, then allows one to compute the coherent Green's function for the average atom.

The BEB formalism [33,34] is a generalization of the CPA such that it becomes applicable also to off-diagonal disorder. Similar to CPA it was formulated for a tight-binding model in which the hopping matrix elements depend on the species of atoms occupying the two sites connected by the hopping. For the above binary alloy example, the BEB hopping matrix elements are t_{AA}, t_{AB}, and t_{BB}. When the hopping matrix elements are equal the BEB formalism reduces to the CPA [14,15], and for the binary alloy case the scalar CPA equation becomes a 2×2 matrix equation. An in-depth analysis of the BEB method was performed in a tight-binding formalism by Gonis and Garland [42] using locators, propagators, and a variational technique proving the analyticity of the BEB-CPA Green's function. A realistic multiband formulation of the BEB-CPA was introduced more than three decades ago by Papaconstantopoulos, Gonis, and Laufer [43]. Then Koepernik *et al.* [37] developed the BEB-CPA extension within a full potential local-orbital approach, and more recently a similar implementation was made within a pseudopotential approach [44]. Shvaika [45] found a connection between the Falicov-Kimball model with correlated hopping and the BEB-CPA by rewriting the Hamiltonian as a 2×2 matrix. For Hamiltonians with interactions the BEB-CPA was employed by Burdin and Fulde [46] to study the interplay between the Kondo effect and disorder. In an attempt to address localization in strongly disordered electronic systems, the typical medium theory [28] was combined with the dynamical cluster approximation including effects induced by off-diagonal disorder [35]. However, this approach did not include electronic interactions.

In the present paper we extend the BEB formalism to *interacting* electrons such that it can be applied to the multicomponent Anderson-Hubbard model; localization effects will not be addressed. The model is defined in Sec. II B. The corresponding DMFT equations are solved using the recently developed fork tensor-product state solver [39].

A. Configurational averages and notation

In the conventional approach to systems with random variables (diagonal and/or off diagonal) the Green's function is first expanded and then an average over an appropriate set of terms is performed. By contrast, the BEB method treats both diagonal- and off-diagonal randomness on equal footing by employing an extended representation, which will be discussed below. The Green's functions are then evaluated using conventional expansion techniques. The formalism introduced by Koepernik *et al.* [37,38] is particularly suitable for the BEB approach. For this reason, we adopt the notation introduced in Refs. [37,38].

We consider an alloy consisting of M types of atoms ("alloy components") denoted by the index α. Every lattice site i is uniquely mapped to a particular component α as expressed by

$$i \mapsto \alpha. \tag{1}$$

While this notation corresponds, in principle, to that of Ref. [38], we reverse the direction of the arrow to focus on the alloy components rather than the lattice sites. To address multiple sites we use the notation $(i, j \mapsto \alpha, \beta) \coloneqq (i \mapsto \alpha) \wedge$

($j \mapsto \beta$). We refer to a specific mapping of the N lattice sites to the M components as a "configuration" (conf) or "disorder realization" and denote the set of all possible configurations by $\mathbb{C} = \{\text{conf}\}$. As the specific configuration of a sample measured in an experiment is unknown, we average over all possible configurations. Since the concentrations c^α of the different components α are assumed to be known we restrict the average to configurations with these concentrations, denoted by $\mathbb{C}|_{\{c^\alpha\}}$. In the absence of additional information we further assume that the probability of all physical configurations is the same:

$$P(\text{conf}) = 1/|\mathbb{C}|_{\{c^\alpha\}}| \quad \forall\ \text{conf} \in \mathbb{C}|_{\{c^\alpha\}}. \tag{2}$$

For a random variable X, the stochastic average over all physical configurations is the weighted sum

$$\mathbb{E}(X) = \sum_{\text{conf}\in\mathbb{C}|_{\{c^\alpha\}}} P(\text{conf}) x_{\text{conf}} = \frac{1}{|\mathbb{C}|_{\{c^\alpha\}}|} \sum_{\text{conf}\in\mathbb{C}|_{\{c^\alpha\}}} x_{\text{conf}}. \tag{3}$$

This situation corresponds to the case of substitutional disorder.

B. Multicomponent Anderson-Hubbard model

For a specific configuration the Anderson-Hubbard Hamiltonian reads

$$\hat{H} = -\sum_{ij\sigma} t_{ij} \hat{c}^\dagger_{i\sigma} \hat{c}_{j\sigma} + \sum_{i\sigma} (v_i - \mu) \hat{n}_{i\sigma} + \sum_i U_i \hat{n}_{i\uparrow} \hat{n}_{i\downarrow}, \tag{4}$$

with the on-site energy v_i, the local Hubbard interaction U_i, and the amplitude t_{ij} for hopping between sites i and j. The hopping parameters are Hermitian $t_{ij} = t^*_{ji}$ and off diagonal, with $t_{ii} = 0$. The Hamiltonian can be written in the compact matrix form

$$\hat{H} = \sum_\sigma \hat{\boldsymbol{c}}^\dagger_\sigma \boldsymbol{H}_\sigma \hat{\boldsymbol{c}}_\sigma + \hat{\boldsymbol{n}}^\intercal_\uparrow \boldsymbol{U} \hat{\boldsymbol{n}}_\downarrow, \tag{5}$$

where we introduced $N \times 1$ matrices to represent the operators. The rows of the matrix $\hat{\boldsymbol{c}}_\sigma$ are the annihilation operators $\hat{c}_{i\sigma}$, and the rows of $\hat{\boldsymbol{n}}_\sigma$ are the number operators $\hat{n}_{i\sigma}$. The one-particle Hamiltonian matrix reads $(\boldsymbol{H})_{ij} = -t_{ij} + \delta_{ij}(v_i - \mu)$. Here and in the following we suppress the spin index σ unless explicitly needed, to simplify the notation. The local interaction is written as a matrix $(\boldsymbol{U})_{ij} = \delta_{ij} U_i$.

The magnitude of the hopping parameters t_{ij} depends on the alloy components located on sites i and j, respectively, which are referred to as terminal points. In the following we employ the "terminal-point approximation" [37,38] which assumes that parameters with terminal points $i, j, k, \ldots$ depend only on the components located at $i, j, k, \ldots$ and not on the components surrounding these sites. Thus, for a specific configuration (disorder realization) every parameter v_i, U_i, and t_{ij} takes a value depending on the component occupying the respective site or sites. In the representation of the BEB we denote these configuration-specific values by an underline and a superscript indicating the component. For instance, if site i is occupied by component α ($i \mapsto \alpha$) the parameter v_i takes the value $\underline{v}^\alpha$. For $i, j \mapsto \alpha, \beta$, we have $v_i = \underline{v}^\alpha$, $U_i = \underline{U}^\alpha$, and $t_{ij} = \underline{t}^{\alpha\beta}(|\mathbf{r}_i - \mathbf{r}_j|)$. This will now be formalized. Denoting the set of sites i occupied by the component α by

$$\mathbb{S}^\alpha \coloneqq \{i | i \mapsto \alpha\}, \tag{6}$$

the terminal point approximation can be expressed conveniently using the indicator function

$$1_{\mathbb{S}^\alpha}(i) \coloneqq \begin{cases} 1 & \text{if} \quad i \in \mathbb{S}^\alpha \\ 0 & \text{if} \quad i \notin \mathbb{S}^\alpha. \end{cases} \tag{7}$$

The identity $\sum_\alpha 1_{\mathbb{S}^\alpha}(i) = 1$ holds since every site must be occupied by exactly one component. Thus, the parameters read

$$v_i = \sum_\alpha 1_{\mathbb{S}^\alpha}(i) \underline{v}^\alpha, \quad t_{ij} = \sum_{\alpha\beta} 1_{\mathbb{S}^\alpha}(i) \underline{t}^{\alpha\beta}(|\mathbf{r}_i - \mathbf{r}_j|) 1_{\mathbb{S}^\beta}(j),$$
$$H_{ij} = \sum_{\alpha\beta} 1_{\mathbb{S}^\alpha}(i) \underline{H}^{\alpha\beta}_{ij} 1_{\mathbb{S}^\beta}(j), \quad U_i = \sum_\alpha 1_{\mathbb{S}^\alpha}(i) \underline{U}^\alpha, \tag{8}$$

with $\underline{H}^{\alpha\beta}_{ij} = \delta_{ij}\delta^{\alpha\beta}(\underline{v}^\alpha - \mu) - \underline{t}^{\alpha\beta}(|\mathbf{r}_i - \mathbf{r}_j|)$. We further note that the conditional expectation value of the parameters equals the underlined component variables:

$$\mathbb{E}(v_i | i \mapsto \alpha) = \underline{v}^\alpha, \quad \mathbb{E}(t_{ij} | i, j \mapsto \alpha, \beta) = \underline{t}^{\alpha\beta}, \ldots. \tag{9}$$

The dependence on the components is therefore shifted from the parameters into the indicator function $1_{\mathbb{S}^\alpha}(i)$. Depending on the component occupying a site, the indicator function selects the corresponding parameter from a finite set of choices. We note that for elements diagonal in lattice sites i, one has $1_{\mathbb{S}^\alpha}(i) 1_{\mathbb{S}^\beta}(i) = 1_{\mathbb{S}^\alpha}(i)\delta^{\alpha\beta}$; i.e., they are diagonal in the components. In the following we refer to a quantity with multiple indices, which include both site and component indices, as a "tensor."

We introduce the indicator tensor

$$\underline{\eta}^\alpha_{ij} = 1_{\mathbb{S}^\alpha}(i)\delta_{ij} =$$

. (10)

Graphically we represent this tensor as a box with legs as seen on the right-hand side of Eq. (10). The order of the tensor is given by the number of its legs, here three. The upper leg carries the alloy component indices α, and the lower legs correspond to the site indices i, j. Within our matrix notation this tensor is equivalent to an $MN \times N$ matrix. We group the left indices for sites i and components α, or in the graphical notation the legs above each other. In the following we refer to the MN-dimensional vector space of grouped sites and components as "extended space." Matrix products in the extended space sum over the grouped MN elements for component and site indices; they are equivalent to the tensor contraction of two legs, one for the component and one for the sites. In this matrix notation the Hamiltonian reads

$$\hat{H} = \sum_\sigma \hat{\boldsymbol{c}}^\dagger_\sigma \underline{\boldsymbol{\eta}}^\intercal \underline{\mathbf{H}}_\sigma \underline{\boldsymbol{\eta}} \hat{\boldsymbol{c}}_\sigma + \hat{\boldsymbol{n}}^\intercal_\uparrow \underline{\boldsymbol{\eta}}^\intercal \underline{\mathbf{U}} \underline{\boldsymbol{\eta}} \hat{\boldsymbol{n}}_\downarrow, \tag{11}$$

where we introduced the local interaction tensor $(\underline{\mathbf{U}})^{\alpha\beta}_{ij} = \delta_{ij} \underline{U}^\alpha \delta^{\alpha\beta}$. In the noninteracting case the Hamiltonian matrix of a specific configuration is the extended matrix sandwiched by the indicator tensors,

$$\boldsymbol{H} = \underline{\boldsymbol{\eta}}^\intercal \underline{\mathbf{H}} \underline{\boldsymbol{\eta}} =$$

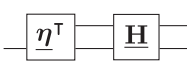

. (12)

TABLE I. Notations specific to the extended basis and Hamiltonian parameters used in BEB method.

$i, j, \ldots$	site indices	c^α	concentration of component α
$\alpha, \beta, \ldots$	alloy components	$\underline{\mathrm{v}}^\alpha$	on-site energy of component α
$i \mapsto \alpha$	mapping of a site to an alloy component	$\underline{\mathrm{U}}^\alpha$	Hubbard parameter of component α
$\mathbb{S}^\alpha$	set of sites occupied by component α	$\underline{\mathrm{t}}^{\alpha\beta}(\lvert\mathbf{r}_i - \mathbf{r}_j\rvert)$	hopping between component α and β
$\mathbb{C}\lvert_{\{c^\alpha\}}$	set of configurations (disorder realization) restricted to given concentrations c^α	$\underline{\mathrm{H}}_{ij}^{\alpha\beta}$	extended Anderson-Hubbard Hamiltonian matrix
		$\underline{\eta}_{ij}^{\alpha}$	indicator tensor, represented as equivalent matrix
X	scalar random variable	$\underline{\boldsymbol{\chi}}$	projector onto specific disorder configuration
$\mathbb{E}(X)$	expectation value defined according to Eq. (3)	$\underline{\mathrm{T}}^{\alpha\beta}$	dimensionless hopping parameter describing hopping between components α and β

In the extended representation, for every lattice site the noninteracting Hamiltonian matrix $\underline{\mathbf{H}}$ is assigned a corresponding element for each component. In this way the noninteracting Hamiltonian can be generated by $\underline{\mathbf{H}}$ for every disorder configuration. The matrix product in the algebraic equation equals the tensor contractions of the internal legs as illustrated by the right-hand side of Eq. (12). Appendix A provides an explicit example for a system of $N = 3$ sites and $M = 2$ components. In Table I we collect the symbols used in our paper.

We note that the only configuration-dependent parts in Eq. (11) are the matrices $\underline{\boldsymbol{\eta}}$ and $\underline{\boldsymbol{\eta}}^\intercal$; the rest are independent of the specific disorder realization. In other words, comparing Eq. (5) with Eq. (11), the configuration dependence of the former equation is moved from the Hamiltonian matrix to the local indicator tensors [Eq. (10)]. This is the main point of the BEB algorithm: One can work with a nonrandom but extended Hamiltonian matrix $\underline{\mathbf{H}}$, which contains the parameters for all possible configurations. A specific configuration can be selected by applying indicator tensors $\underline{\boldsymbol{\eta}}$. What remains to be averaged over are these local indicator tensors.

1. Alloy component Green's function

In the absence of interaction, $\underline{\mathbf{U}} = 0$, the model can be solved by the generalized CPA introduced by Blackman, Esterling, and Berk [33,34]. Using the indicator tensor $\underline{\boldsymbol{\eta}}$ [Eq. (10)] we define the projector:

$$\underline{\boldsymbol{\chi}} = \underline{\boldsymbol{\eta}}\underline{\boldsymbol{\eta}}^\intercal = \quad ; \qquad \underline{\boldsymbol{\chi}}^2 = \underline{\boldsymbol{\chi}}. \tag{13}$$

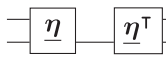

It maps a vector in the extended space onto a single configuration; all elements corresponding to different configurations are set to zero. The projector property follows from the indicator identity $\underline{\boldsymbol{\eta}}^\intercal\underline{\boldsymbol{\eta}} = \mathbb{1}$. We define the component Green's function as

$$\underline{\mathbf{G}}(z) := \underline{\boldsymbol{\eta}}\boldsymbol{G}(z)\underline{\boldsymbol{\eta}}^\intercal = \quad ; \qquad \sum_{\alpha\beta}\underline{\mathbf{G}}^{\alpha\beta}(z) = \boldsymbol{G}(z). \tag{14}$$

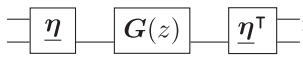

The arrangement of indicator tensors $\underline{\boldsymbol{\eta}}$ is different compared to Eq. (12): Both the Green's function $\boldsymbol{G}$ and the component Green's function $\underline{\mathbf{G}}$ are configuration dependent. We note that local elements are diagonal in component space, i.e., $\underline{\mathrm{G}}_{ii}^{\alpha\beta}(z) \propto \delta^{\alpha\beta}$. For the noninteracting system, we sandwich the resolvent for the Green's function

$$\mathbb{1} = [\mathbb{1}z - \boldsymbol{H}]\boldsymbol{G}(z) \tag{15}$$

by $\underline{\boldsymbol{\eta}}$ from the left and $\underline{\boldsymbol{\eta}}^\intercal$ from the right; this yields the equation for the component Green's function,

$$\underline{\boldsymbol{\chi}} = [\mathbb{1}z - \underline{\boldsymbol{\chi}}\underline{\mathbf{H}}\underline{\boldsymbol{\chi}}]\underline{\mathbf{G}}(z). \tag{16}$$

The law of total probability [47] relates the average of the component Green's functions $\underline{\mathrm{G}}_{ij}^{\alpha\beta}$ and the conditional average of the physical Green's function G_{ij} in the following way:

$$\mathbb{E}\big(\underline{\mathrm{G}}_{ij}^{\alpha\beta}\big) = \begin{cases} c^\alpha\mathbb{E}(G_{ii}(z)|i \mapsto \alpha)\delta^{\alpha\beta} & \text{for} \quad i = j \\ c^\alpha c^\beta\mathbb{E}(G_{ij}(z)|i, j \mapsto \alpha, \beta) & \text{for} \quad i \neq j. \end{cases} \tag{17}$$

2. Effective medium in the extended space

As in the CPA, in the BEB formalism one calculates an effective local Green's function $\underline{\mathbf{g}}_{\mathrm{loc}}(z)$ from an effective medium $\underline{\mathbf{S}}(z)$, which approximates the average local Green's function $\mathbb{E}(\underline{\mathbf{G}}_{ii}(z))$. We consider only substitutional disorder without structural disorder; i.e., the lattice structure is assumed to be fixed. Therefore, we decompose the hopping tensor $\underline{\mathrm{t}}^{\alpha\beta}(\lvert\mathbf{r}_i - \mathbf{r}_j\rvert)$ into its component part, $\underline{\mathrm{T}}^{\alpha\beta}$, and its lattice part, $t(\lvert\mathbf{r}_i - \mathbf{r}_j\rvert)$:

$$\underline{\mathrm{t}}^{\alpha\beta}(\lvert\mathbf{r}_i - \mathbf{r}_j\rvert) =: \underline{\mathrm{T}}^{\alpha\beta}\,t(\lvert\mathbf{r}_i - \mathbf{r}_j\rvert). \tag{18}$$

Depending on the component of the end points, the matrix elements $\underline{\mathrm{T}}^{\alpha\beta}$ scale the amplitudes for hopping on a given lattice structure by a dimensionless factor. In the following we refer to $\underline{\mathrm{T}}^{\alpha\beta}$ simply as a "dimensionless hopping parameter." We perform the lattice Fourier transform for the hopping matrix elements as

$$\underline{\mathbf{T}}\frac{1}{N}\sum_{ij}t(\lvert\mathbf{r}_i - \mathbf{r}_j\rvert)e^{i\mathbf{k}\cdot(\mathbf{r}_i - \mathbf{r}_j)} = \underline{\mathbf{T}}\epsilon_k. \tag{19}$$

For a given effective medium $\underline{\mathbf{S}}(z)$, the effective local Green's function reads

$$\underline{\mathbf{g}}_{\mathrm{loc}}(z) = \frac{1}{N}\sum_k[\mathbb{1}z - \underline{\mathbf{S}}(z) - \underline{\mathbf{T}}\epsilon_k]^{-1}. \tag{20}$$

The effective medium as well as the effective local Green's function are represented by $M \times M$ matrices in the components. Being local quantities they no longer carry lattice indices. The effective medium $\underline{\mathbf{S}}(z)$ is determined by

demanding that the averaged $\mathbf{t}$ matrix vanishes:

$$\mathbb{E}\big(\mathbf{t}(z)\big) \stackrel{!}{=} 0, \tag{21}$$

$$\mathbf{t}(z) \coloneqq -[\underline{\boldsymbol{\chi}}[\mathbb{1} - \underline{\boldsymbol{\chi}}(\mathbb{1}z - \underline{\mathbf{S}}(z) + \underline{\mathbf{v}})\underline{\boldsymbol{\chi}}]^{-1}\underline{\boldsymbol{\chi}} + \underline{\mathbf{g}}_{\mathrm{loc}}(z)]^{-1}. \tag{22}$$

C. Inclusion of electronic interactions and the BEB+DMFT self-consistency loop

We treat the local Hubbard interaction within the dynamical mean-field theory [20,23,24], which assumes a local self-energy $\Sigma_{ij}(z) = \delta_{ij}\Sigma_{ii}(z)$; this property becomes exact in the limit of infinite coordination number. The problem of interacting disordered electrons may equally be viewed as a system of noninteracting particles moving in an effective local, energy-dependent potential $\Sigma_{ii}(z)$ (for details see Refs. [26,48]). The DMFT self-consistency equations [23] are equivalent to a fixed-point problem which can be expressed by a functional $\widehat{\Sigma}$: Given a self-energy Σ_{ii} and the resulting local Green's function $G_{ii}(\Sigma_{ii})$ this functional provides a new self-energy $\widehat{\Sigma}[G_{ii}(\Sigma_{ii}), \Sigma_{ii}]$, such that the DMFT self-energy is determined self-consistently by the fixed point

$$\Sigma_{ii} = \widehat{\Sigma}[G_{ii}(\Sigma_{ii}), \Sigma_{ii}]. \tag{23}$$

Within the CPA, the local Green's function for a given self-energy $G_{ii}(\Sigma_{ii})$ is replaced by the conditional average $\mathbb{E}(G_{ii}(\Sigma_{ii})|i \mapsto \alpha) = \underline{g}^{\alpha\alpha}_{\mathrm{loc}}(\Sigma_{ii})/c^{\alpha}$ [see Eqs. (17) and (20)]. Thus, the self-energy $\widehat{\Sigma}[\underline{g}^{\alpha\alpha}_{\mathrm{loc}}(\Sigma_{ii})/c^{\alpha}, \Sigma_{ii}]$ depends on the component α. Consequently, the self-energy at the fixed point depends on the component α, but not on the explicit site i:

$$\Sigma^{\alpha} = \widehat{\Sigma}\big[\underline{g}^{\alpha\alpha}_{\mathrm{loc}}(\Sigma^{\alpha})/c^{\alpha}, \Sigma^{\alpha}\big]. \tag{24}$$

This allows one to introduce the BEB+DMFT self-consistency which we will discuss next.

By merging the BEB formalism with DMFT a twofold self-consistency arises, one for the BEB and one for the DMFT corresponding to the fixed-point Eq. (24). The self-consistency equation of the BEB formalism is pointwise in the frequencies and is therefore much simpler than the self-consistency condition of the DMFT, where frequencies mix due to the energy exchange caused by the interaction between the electrons. We view the former self-consistence as an internal part of the full self-consistency loop. In the BEB method we calculate an effective local Green's function $\underline{\mathbf{g}}_{\mathrm{loc}}(z)$, Eq. (20). The effective medium $\underline{\mathbf{S}}(z)$ and, therefore, the effective local Green's function have to be calculated self-consistently from Eqs. (21) and (22). This condition simplifies to

$$\underline{\mathbf{g}}^{-1}_{\mathrm{loc}}(z) = \overline{\underline{\mathbf{g}}}^{-1}(z) \tag{25}$$

with the diagonal matrix

$$\overline{\underline{g}}^{\alpha\beta}(z) = \frac{c^{\alpha}\delta^{\alpha\beta}}{\big(\underline{\mathbf{g}}^{-1}_{\mathrm{loc}}\big)^{\alpha\alpha}(z) + \underline{S}^{\alpha\alpha}(z) + \mu - \underline{v}^{\alpha} - \Sigma^{\alpha}(z)}, \tag{26}$$

where $\Sigma^{\alpha}(z)$ is the DMFT self-energy for the component α. The self-consistent Eq. (25) can be solved with standard root-search algorithms or by simple iteration. In practice, we use an implementation of the BEB formalism without interactions and merely shift the on-site energy $\underline{v}^{\alpha} \to \underline{v}^{\alpha} + \Sigma^{\alpha}(z)$. An efficient evaluation of the BEB self-consistency equation is discussed in Appendix B; an implementation is provided in Ref. [49]. To emphasize the dependence on the self-energy we denote the self-consistently determined effective local Green's function for a given self-energy, Eq. (25), by $\underline{\mathbf{g}}_{\mathrm{loc}}(z, \boldsymbol{\Sigma}(z))$.

With the BEB self-consistency condition, Eq. (25), for the local Green's function $\underline{\mathbf{g}}_{\mathrm{loc}}(z, \boldsymbol{\Sigma}(z))$, the combined algorithm corresponds to the conventional DMFT self-consistency condition, Eq. (24), where the local Green's function, calculated from the lattice Hilbert transform, is now replaced by the average

$$\mathbb{E}(G_{ii}|i \mapsto \alpha) = \underline{g}^{\alpha\alpha}_{\mathrm{loc}}(z, \boldsymbol{\Sigma}(z))/c^{\alpha}.$$

The reciprocal concentration factor can be avoided by introducing a renormalized indicator tensor, which leads to a slightly modified BEB self-consistency as elaborated in Appendix C. We have to solve a separate impurity problem for every component α. Starting from an initial guess for the DMFT self-energy $\Sigma^{\alpha}(z)$ for every component, the BEB+DMFT scheme is the following:

(1) Calculate the effective local Green's function [Eq. (20)] using Eqs. (25) and (26), which yields

$$\underline{\mathbf{g}}_{\mathrm{loc}}(z, \boldsymbol{\Sigma}(z)). \tag{27a}$$

(2) Calculate the hybridization function

$$\Delta^{\alpha}(z) = z + \mu - \underline{v}^{\alpha} - \Sigma^{\alpha}(z) - c^{\alpha}/\underline{g}^{\alpha\alpha}_{\mathrm{loc}}(z, \boldsymbol{\Sigma}(z)), \tag{27b}$$

for every component α.

(3) Solve the impurity problem for the self-energy

$$\Sigma^{\alpha}(z) = \Sigma[\underline{v}^{\alpha}, \underline{U}^{\alpha}, \Delta^{\alpha}] \tag{27c}$$

for every component α.

(4) Repeat from step 1 until self-consistency is reached.

The hybridization function can also be expressed in terms of BEB quantities using the self-consistency condition, Eq. (25):

$$\Delta^{\alpha}(z) = z - \underline{S}^{\alpha\alpha}(z) - \big(\underline{\mathbf{g}}^{-1}_{\mathrm{loc}}\big)^{\alpha\alpha}(z, \boldsymbol{\Sigma}(z)). \tag{28}$$

This is different from CPA+DMFT, where only one unique hybridization function exists independent of the alloy components. Analogous to the nondisordered case, an expression for the hybridization function of the Bethe lattice in terms of the local Green's function $\underline{\mathbf{g}}_{\mathrm{loc}}(z, \boldsymbol{\Sigma}(z))$ is given in Appendix D.

Central to the DMFT problem is the impurity solver which provides the local dynamic self-energy, Eq. (27c). To this end, we employ a tensor-network-based zero-temperature solver, the fork tensor-product state (FTPS) solver [39]. The FTPS impurity solver is a Hamiltonian-based method which discretizes the hybridization function, Eq. (27b), using a large number of bath sites. We use 249 sites per spin, resulting in a median energy distance of $0.03D$, where the half bandwidth D sets our energy scale. We calculate the ground state $|GS\rangle$ of the finite size impurity problem using the density matrix renormalization group (DMRG) [50,51]. Subsequently, we perform the time evolution using the time-dependent variational principle (TDVP) [52–55]. To obtain the retarded time impurity Green's function $G^{\mathrm{ret}}(t)$, the states $\hat{c}_{\sigma}|GS\rangle$, $\hat{c}^{\dagger}_{\sigma}|GS\rangle$, as well as their adjoint states are time evolved, where $\hat{c}_{\sigma}$ ($\hat{c}^{\dagger}_{\sigma}$) is the annihilation (creation) operator of the impurity site. For DMRG we chose a truncated weight of 10^{-15} and a maximal

bond dimension of 100. We perform the TDVP using time steps of $0.1/D$ up to a maximal time $t_{\max} = 150/D$ with a truncated weight of 10^{-9} and a maximal bond dimension of 150. The convergence with respect to these parameters is checked.

We can calculate the Green's function $G^{\text{ret}}(t)$ only up to a maximal time, and we have (small) finite size effects due to the discretization of the bath. Therefore, we cannot evaluate the retarded Green's function directly on the real-frequency axis $G(\omega + i0^+)$. Instead we calculate it on a parallel contour $G(\omega + i\eta)$ shifted by a fixed finite $\eta > 0$; this corresponds to the Laplace transform:

$$G(\omega + i\eta) = \int_0^\infty dt e^{i(\omega+i\eta)t} G^{\text{ret}}(t) =: \mathrm{F}_\eta[G^{\text{ret}}(t)](\omega). \quad (29)$$

The shift η acts as a broadening for the Green's function $G(z)$ as can be seen from the Cauchy integral formula

$$2\pi i G(\omega + i\eta) = \oint dz \frac{G(z)}{z - \omega - i\eta} = \int_{-\infty}^{\infty} d\omega' \frac{G(\omega' + i0^+)}{\omega' - \omega - i\eta^-}, \quad (30)$$

with $\eta^- = \eta - 0^+$, where 0^+ is a positive infinitesimal. We write the Green's function on the real axis in terms of the shifted Fourier transform,

$$\begin{aligned} G(\omega + i0^+) &= \lim_{\eta' \searrow 0} \mathrm{F}_{\eta'}[G^{\text{ret}}(t)](\omega) = \mathrm{F}_\eta[e^{t\eta^-} G^{\text{ret}}(t)](\omega) \\ &= \sum_k \frac{1}{k!} (\eta^-)^k \mathrm{F}_\eta[t^k G^{\text{ret}}(t)](\omega). \end{aligned} \quad (31)$$

The second equality replaces the limit $\eta' \searrow 0$ using $\lim_{\eta' \searrow 0} \exp(-\eta' t) = \exp(-\eta t)\exp(\eta^- t)$ introducing a finite variable η; in the last line we use the series representation of the exponential function $\exp(\eta^- t)$. The first term $k = 0$ is the Green's function on the shifted contour $G(\omega + i\eta)$; higher-order terms give systematic corrections. In Sec. III, we calculate the first-order correction

$$G(\omega + i0^+) = G(\omega + i\eta) + \eta \mathrm{F}_\eta[t G^{\text{ret}}(t)](\omega) + \mathcal{O}(\eta^2) \quad (32)$$

with a typical shift $\eta = 0.08$. The self-energy is calculated from the equation of motion of the impurity model [56],

$$\Sigma_\sigma(z) = U F_\sigma(z)/G_\sigma(z), \quad (33)$$

$$F^{\text{ret}}(t) = \langle GS | \hat{c}_\sigma(t) \hat{n}_{-\sigma}(t) \hat{c}_\sigma^\dagger | GS \rangle, \quad (34)$$

where $F(z)$ is the Laplace transform of $F^{\text{ret}}(t)$.

D. General properties of the BEB formalism

We shortly review some properties of the BEB formalism [19,38,42]. First, the BEB formalism is equivalent to the CPA when off-diagonal disorder is absent. This limit was already proven in the original formulation [33,34]. Since the BEB theory includes the off-diagonal disorder in the single-site approximation, the Herglotz property [57,58] of the CPA is preserved in the BEB as well [42].

Second, for a noninteracting tight-binding Hamiltonian the density of states (DOS) is nonzero only within certain energy ranges, determined by the Hamiltonian matrix elements. This also holds for the CPA [16]. Koepernick *et al.* [38] found the same in their numerical study of one-dimensional chains using the BEB formalism. Likewise, we find no violations of this property in our numerical results. In the following section we derive exact bounds for the spectral function of a Bethe lattice with coordination number Z using the BEB formalism in the limit of independent alloy components, i.e., when there is no hopping between different components.

E. Limit of independent components

We consider the limit of vanishing hopping between different components. If the hopping is diagonal in the components, $\underline{\mathrm{T}}^{\alpha\beta} \propto \delta^{\alpha\beta}$, the BEB effective medium $\underline{\mathbf{S}}(z)$ is also diagonal in the components and the self-consistency equations [Eq. (25)] decouple. In this case, the effective local Green's function, Eq. (20), can be readily calculated, since the matrix inverse is the reciprocal of the diagonal elements:

$$\underline{\mathrm{g}}^{\alpha\beta}_{\text{loc}}(z) = \frac{1}{N} \sum_k \frac{\delta^{\alpha\beta}}{z - \underline{\mathrm{S}}^{\alpha\alpha}(z) - \underline{\mathrm{T}}^{\alpha\alpha}\epsilon_k} = \delta^{\alpha\beta} g_0^\alpha(z - \underline{\mathrm{S}}^{\alpha\alpha}(z)). \quad (35)$$

Here, g_0^α is the lattice Hilbert transform $g_0(z) = \frac{1}{N}\sum_k \frac{1}{z-\epsilon_k}$; the superscript α indicates that the bandwidth is scaled by $\underline{\mathrm{T}}^{\alpha\alpha}$:

$$g_0^\alpha(z) = \frac{1}{N} \sum_k \frac{1}{z - \underline{\mathrm{T}}^{\alpha\alpha}\epsilon_k} = \frac{1}{\underline{\mathrm{T}}^{\alpha\alpha}} g_0(z/\underline{\mathrm{T}}^{\alpha\alpha}). \quad (36)$$

For the component α, the decoupled self-consistency, Eq. (25), reads

$$0 = \frac{\overline{c}^\alpha}{g_0^\alpha(z - \underline{\mathrm{S}}^{\alpha\alpha})} + \underline{\mathrm{S}}^{\alpha\alpha} - \underline{\mathrm{v}}^\alpha, \quad (37)$$

with the concentration complement $\overline{c}^\alpha = 1 - c^\alpha \geqslant 0$. For a Bethe lattice with coordination number Z and the lattice Hilbert transform [18]

$$g_0(z, Z) = 2(Z-2)/[z(Z - 2 + Z\sqrt{1 - D^2/z^2})], \quad (38)$$

where D is the half bandwidth, the self-consistency condition is an algebraic equation and can be solved analytically. The BEB effective medium reads

$$\underline{\mathrm{S}}^{\alpha\alpha}(z, Z) = \frac{(Z-2)\underline{\mathrm{v}}^\alpha c^\alpha + Z\underline{\mathrm{v}}^\alpha + (Z+2)c^\alpha z - Zz - 2(c^\alpha)^2 z - Z\overline{c}^\alpha s\sqrt{(z - \underline{\mathrm{v}}^\alpha)^2 - c^\alpha (D^\alpha)^2 \frac{Z - c^\alpha}{Z-1}}}{2c^\alpha(Z - c^\alpha)}, \quad (39)$$

where s is the sign $s = \text{sign}(\text{Re}\,(z - v^\alpha))$, and D^α is the half bandwidth scaled by $\underline{\mathrm{T}}^{\alpha\alpha}$; this is the retarded solution. A conjugate solution exists with $-s$ and therefore with a plus sign in front of the square root.

We are interested in the bandwidth of the resulting component spectrum,

$$A^\alpha(\omega) = -\frac{1}{c^\alpha \pi}\mathrm{Im}\, g_0^\alpha(\omega + i0^+ - \underline{\mathrm{S}}^{\alpha\alpha}(\omega + i0^+)). \quad (40)$$

For noninteracting systems, the Gershgorin circle theorem [59] gives the *maximal* spectral bounds

$$|z - \underline{\mathrm{v}}^\alpha| \leqslant D^\alpha. \quad (41)$$

In the limit $\underline{\mathrm{T}}^{\alpha\beta} \propto \delta^{\alpha\beta}$, we can make a more precise statement and derive exact spectral bounds as will be discussed below. The spectral function can only vanish when the imaginary part of the effective medium vanishes. Thus, for noninteracting systems, we need to check where the argument of the square root is negative. One finds an imaginary part and therefore spectral weight for

$$|z - \underline{\mathrm{v}}^\alpha| < \sqrt{c^\alpha \frac{Z - c^\alpha}{Z-1}} D^\alpha. \quad (42)$$

Therefore, for the Bethe lattice with coordination number Z and $\underline{\mathrm{T}}^{\alpha\beta} \propto \delta^{\alpha\beta}$, the bandwidth is reduced due to concentration by a factor $\sqrt{c^\alpha(Z - c^\alpha)/(Z-1)}$. We then obtain the effective bandwidth

$$D^\alpha_{\mathrm{eff}} = \sqrt{c^\alpha \frac{Z - c^\alpha}{Z-1}} \underline{\mathrm{T}}^{\alpha\alpha} D. \quad (43)$$

Our numerical results in Sec. III were obtained for a semicircular DOS, i.e., the Bethe lattice with infinite coordination number $Z \to \infty$. In this limit one finds an effective bandwidth

$$D^\alpha_{\mathrm{eff}} = \sqrt{c^\alpha}\underline{\mathrm{T}}^{\alpha\alpha} D. \quad (44)$$

The same factor $\sqrt{c}$ was found in Ref. [60] in the CPA ($\underline{\mathrm{T}}^{\mathsf{AA}} = \underline{\mathrm{T}}^{\mathsf{AB}} = \underline{\mathrm{T}}^{\mathsf{BB}} = 1$) in the limit of high disorder strength, $(\underline{\mathrm{v}}^{\mathsf{B}} - \underline{\mathrm{v}}^{\mathsf{A}})/D = \delta \gg \max(1, U/D)$. While the parameters in these limits are different, both describe the same physics, namely, the decoupling of components. Indeed, the components decouple not only for vanishing hopping between the components $\underline{\mathrm{T}}^{\mathsf{AB}} = 0$, but also in the case of a large separation in energy ($\delta \gg 1$).

For coordination number $Z = 2$ another interesting limit of the Bethe lattice is obtained; this is the one-dimensional (1D) lattice [18], where

$$g_0^{\mathrm{1D}}(z) = g_0(z, Z = 2) = 1/[z\sqrt{1 - D^2/z^2}]. \quad (45)$$

The spectral bounds are given by

$$D^\alpha_{\mathrm{eff}} = \sqrt{c^\alpha(2 - c^\alpha)}\underline{\mathrm{T}}^{\alpha\alpha} D. \quad (46)$$

Therefore, for the one-dimensional lattice and $\underline{\mathrm{T}}^{\alpha\beta} \propto \delta^{\alpha\beta}$ the bandwidth is reduced by the factor $\sqrt{c^\alpha(2 - c^\alpha)}$.

III. NUMERICAL RESULTS

The above formalism is now used to study the effect of off-diagonal disorder in the Anderson-Hubbard model at zero temperature. We employ a Bethe lattice with infinite coordination number, whose half bandwidth D sets the energy scale. Furthermore, we consider a discrete binary random alloy distribution with components A and B.

In all applications we consider the case of half filling on average $\mathbb{E}(n_i) = 1$; this leads to a fixed chemical potential

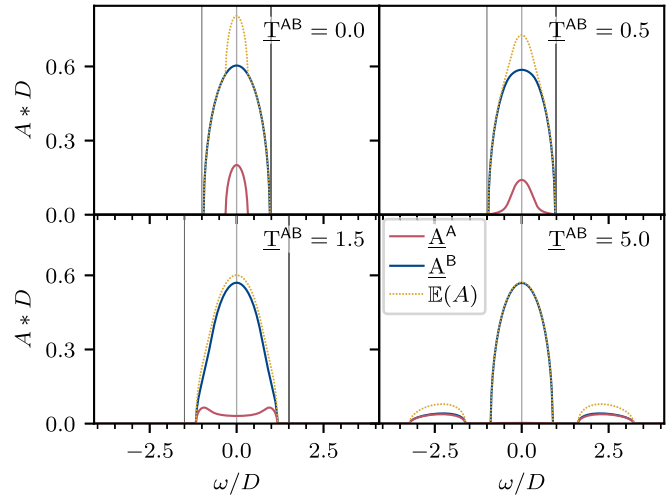

FIG. 1. Noninteracting case: Comparison of spectral functions for different dimensionless hopping parameters $\underline{\mathrm{T}}^{\mathsf{AB}}$. The parameters are $\underline{\mathrm{U}}^{\mathsf{A}} = \underline{\mathrm{U}}^{\mathsf{B}} = 0$, $\underline{\mathrm{v}}^{\mathsf{A}} = \underline{\mathrm{v}}^{\mathsf{B}} = 0$, $c^{\mathsf{A}} = 0.1 = 1 - c^{\mathsf{B}}$, and $\underline{\mathrm{T}}^{\mathsf{AA}} = \underline{\mathrm{T}}^{\mathsf{BB}} = 1$. The solid lines represent the component spectral functions $\underline{\mathrm{A}}^\alpha(z) = c^\alpha \mathbb{E}(A_i(z)|i \mapsto \alpha)$, where A is red and B is blue; the dotted yellow line shows the average spectral function $\mathbb{E}(A(z)) = \underline{\mathrm{A}}^{\mathsf{A}}(z) + \underline{\mathrm{A}}^{\mathsf{B}}(z)$. The thin vertical lines show the maximal spectral bounds given by the Gershgorin circle theorem [59].

which we choose as $\mu = 0$. In the following section we fix the alloy component concentration and study the change in the spectral function starting with the noninteracting case and equal atomic potentials. The alloy component spectral functions are the concentration-weighted conditional spectral functions

$$\underline{\mathrm{A}}^\alpha(\omega) := -\frac{1}{\pi}\mathrm{Im}\, \underline{\mathrm{g}}^{\alpha\alpha}_{\mathrm{loc}}(\omega) = -\frac{c^\alpha}{\pi}\mathrm{Im}\, \mathbb{E}(G_{ii}(\omega)|i \mapsto \alpha). \quad (47)$$

The average spectral functions are given by the trace

$$\mathbb{E}(A(\omega)) = \sum_\alpha \underline{\mathrm{A}}^\alpha(\omega) = -\frac{1}{\pi}\mathrm{Im}\,\mathrm{Tr}\, \underline{\mathbf{g}}_{\mathrm{loc}}(\omega). \quad (48)$$

A. Noninteracting limit

We start with the noninteracting case by setting $\underline{\mathrm{U}}^{\mathsf{A}} = \underline{\mathrm{U}}^{\mathsf{B}} = 0$, which corresponds to the Anderson disorder model with purely off-diagonal disorder. Since the noninteracting Green's function is independent of temperature the results presented in this section are valid not only for zero, but also for finite temperatures. We choose the parameters

$$\underline{\mathrm{v}}^{\mathsf{A}} = \underline{\mathrm{v}}^{\mathsf{B}} = -U/2 = 0, \quad c^{\mathsf{A}} = 0.1 = 1 - c^{\mathsf{B}},$$
$$\underline{\mathrm{T}}^{\mathsf{AA}} = \underline{\mathrm{T}}^{\mathsf{BB}} = 1,$$

and calculate the average and the alloy component spectral functions for several values of $\underline{\mathrm{T}}^{\mathsf{AB}}$ at half filling. The case $\underline{\mathrm{T}}^{\mathsf{AB}} = 1$ is equivalent to the nondisordered case since $\underline{\mathrm{v}}^{\mathsf{A}} = \underline{\mathrm{v}}^{\mathsf{B}}$; in this case the components are indistinguishable. Thus, the average spectral function is just the spectral function of the nondisordered Bethe lattice, and the component Green's function is proportional with a concentration prefactor.

Figure 1 shows the spectral function for off-diagonal disorder with $\underline{\mathrm{T}}^{\mathsf{AB}} = 0.0, 0.5, 1.5, 5.0$. The case $\underline{\mathrm{T}}^{\mathsf{AB}} = 0$ was

solved exactly in Sec. II E. The panel $\underline{T}^{AB} = 0$ in Fig. 1 indicates that off-diagonal disorder reduces the bandwidths; according to Eq. (43) the effective bandwidths are given by $D^{A}_{\text{eff}} = \sqrt{0.1}D \approx 0.32D$ and $D^{B}_{\text{eff}} = \sqrt{0.9}D \approx 0.95D$. For $\underline{T}^{AB} < 1 = \underline{T}^{\alpha\alpha}$ the probabilities for hopping between the alloy components A and B are less than those between the same component α. The spectral functions in the upper half of Fig. 1 correspond to this situation. In spite of a similar support on the energy axis, the spectral function of the majority component B has a larger bandwidth, which encompasses the effective bandwidth of component A. By contrast, when $\underline{T}^{AB} > 1 = \underline{T}^{\alpha\alpha}$, A-B bonds are energetically favorable. The panel $\underline{T}^{AB} = 1.5$ in Fig. 1 shows that the spectral function of component A develops shoulders although both components have similar effective bandwidths. When the value of $\underline{T}^{AB}$ is increased further the shoulders split off from the central band; for the parameters chosen the split-off is visible for $\underline{T}^{AB} \geqslant 2.25$. According to Burdin and Fulde [46] the split-off upper and lower bands correspond to bonding and antibonding states, respectively. In the particle-hole symmetric case, the bonding and antibonding bands in panel $\underline{T}^{AB} = 5.0$ of Fig. 1 have equal weights. Due to the large value $\underline{T}^{AB} = 5.0$, the minority component A is completely suppressed in the central band. The components A and B contribute roughly equally to the bonding and antibonding subbands. Therefore, the central band of the average spectral function is depleted by an amount of $(1 - 2c^{A}) = 0.8$. The overall results and the spectral weight transfer from the central band are consistent with those reported in Ref. [46].

B. Alloy components with equal interaction strengths $\underline{U}^{A} = \underline{U}^{B}$

In the following, we will discuss the results for the interacting case using the setup described in Sec. III A at zero temperature ($T = 0$). The alloy components have identical on-site interaction parameters:

$$\underline{U}^{A} = \underline{U}^{B} = U = 3D.$$

At half filling, the on-site energies are $\underline{v}^{A} = \underline{v}^{B} = -U/2 = -1.5D$.

Figure 2 shows the spectral function for various values of $\underline{T}^{AB}$. For $\underline{T}^{AB} = 0$, when the self-consistency equations decouple, the spectral function of both components implies insulating behavior due to the strong interaction $U = 3D$. The upper and lower Hubbard bands centered around $\pm U/2$ are visible. The bandwidth of the Hubbard bands is effectively reduced according to Eq. (43). Therefore, the gap is wider for component A. Finite values of $\underline{T}^{AB}$ lead to wider spectral functions, and the bandwidth of the minority component A broadens to the same bandwidth as for B. Although for $\underline{T}^{AB} = 1.5$ the imaginary part of the self-energy shows a prominent peak at $\omega = 0$, the spectral function remains finite at the Fermi level. The convergence of the DMFT computations slows down for this value of $\underline{T}^{AB} = 1.5$, hinting at the proximity of a transition. The minority component A exhibits shoulders at the band edge. For $\underline{T}^{AB} = 1.7$ (not shown) one observes a pronounced quasiparticle peak at the Fermi level of both components, indicating that the system is metallic. A further increase to $\underline{T}^{AB} = 5.0$ leads to an increased spectral weight

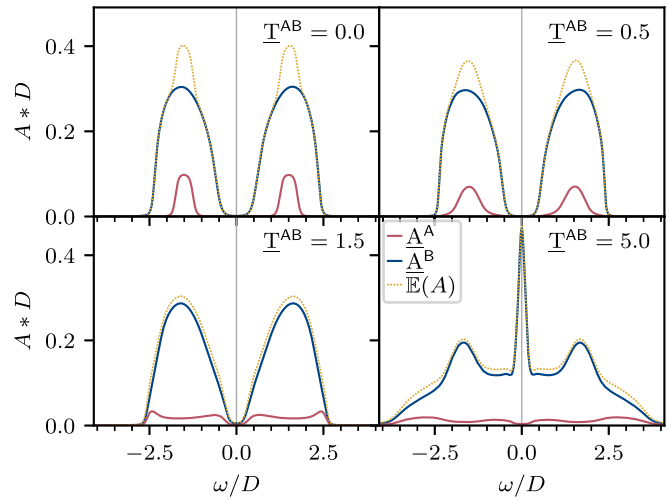

FIG. 2. Comparison of spectral functions for different values of the dimensionless hopping parameter $\underline{T}^{AB}$ with $\underline{U}^{A} = \underline{U}^{B} = 3D$, $\underline{v}^{A} = \underline{v}^{B} = -1.5D$, $c^{A} = 0.1 = 1 - c^{B}$, and $\underline{T}^{AA} = \underline{T}^{BB} = 1$ at $T = 0$. For $\underline{T}^{AB} = 0$ a shift $\eta = 0.12$ had to be used; the other panels were calculated for $\eta = 0.08$.

at the Fermi level for the majority component B, while the spectral function of A has a minimum at the Fermi level.

For small values of $\underline{T}^{AB}$ the spectral gap results from the local Hubbard physics. Disorder then plays a minor role and mostly modifies the bandwidth and therefore the gap size. An increase of $\underline{T}^{AB}$ leads to a larger bandwidth compared to that of the CPA+DMFT result for $\underline{T}^{AB} = 1$. For larger values of $\underline{T}^{AB}$ the spectral function of the component A is seen to open a pseudogap around the Fermi level which is accompanied by an increase of spectral weight of the component B. For large $\underline{T}^{AB}$, the pseudogap is a result of the off-diagonal disorder.

C. Alloy components with different interaction strengths

In a binary alloy the strength of the interaction between electrons may also depend on the alloy component. Therefore, we explore the effect of off-diagonal disorder in this case. We illustrate the results for an extreme case, namely, for a strong repulsion $\underline{U}^{B} = 3D$ of the majority component B only, while the minority component remains noninteracting ($\underline{U}^{A} = 0$). We consider half filling with $\underline{v}^{A} = 0$, $\underline{v}^{B} = -\underline{U}^{B}/2 = -1.5D$ and note that, in spite of the different values $\underline{v}^{A} \neq \underline{v}^{B}$, the effective (diagonal) disorder strength is zero, since the Hartree self-energy compensates the difference.

Figure 3 shows the evolution of the spectral function for increasing $\underline{T}^{AB}$. For $\underline{T}^{AB} = 0$, the A alloy component is metallic, while due to the large $\underline{U}^{B}$ value the B component is insulating. We note that the two components have different effective bandwidths due to the different concentrations. The panel with $\underline{T}^{AB} = 0.5$ shows a small peak for the B component, in spite of the large interaction strength. At $\underline{T}^{AB} = 1$, the A-A, A-B, and B-B hopping probabilities are the same, which leads to the same effective bandwidths, and to the appearance of the metallic state for both alloy components.

In Fig. 3 the panel with $\underline{T}^{AB} = 1.5$ shows a distinct peak for the majority component B at the Fermi level, which reduces the spectral function for the A component at the Fermi level,

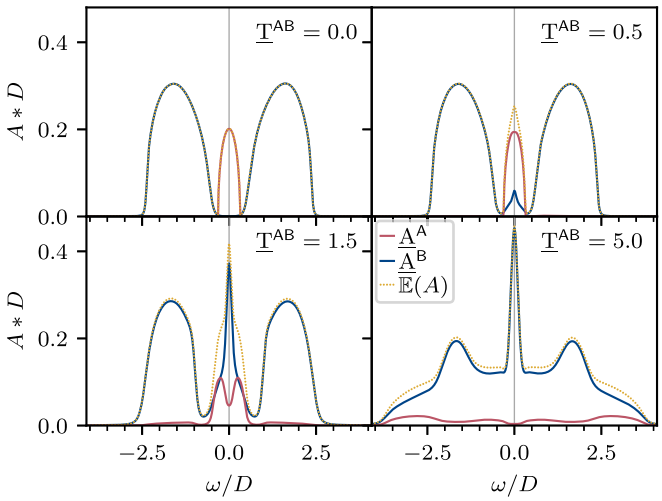

FIG. 3. Comparison of spectral functions for different values of the dimensionless hopping parameter $\underline{T}^{AB}$ with $\underline{U}^{A} = 0$, $\underline{U}^{B} = 3D$, $\underline{v}^{A} = 0$, $\underline{v}^{B} = -1.5D$, $c^{A} = 0.1 = 1 - c^{B}$, and $\underline{T}^{AA} = \underline{T}^{BB} = 1$ at $T = 0$.

leading to a local minimum. Increasing the intercomponent hopping to $\underline{T}^{AB} = 5.0$, the peak of B becomes even larger, and the spectral weight of A almost vanishes at the Fermi level. The panels with $\underline{T}^{AB} = 5.0$ of Figs. 2 and 3 are seen to be very similar; apparently the interaction of the minority component has little effect on the spectral function.

Figure 4 shows the quasiparticle weight

$$Z^{\alpha} = \left[1 - \left.\frac{\partial\, \mathrm{Re}\, \Sigma^{\alpha}(\omega + i\eta)}{\partial \omega}\right|_{\omega=0}\right]^{-1} \tag{49}$$

corresponding to the spectral functions of panel $\underline{T}^{AB} = 5.0$ in Figs. 2 and 3. In spite of the large value of $\underline{U}^{A} = 3D$, the quasiparticle weight Z^{A} is large, with a magnitude around 0.9. This gives an indication why the panels $\underline{T}^{AB} = 5.0$ of Figs. 2 and 3 are so similar; the large value of $\underline{U}^{A} = 3D$ leads only to a small mass renormalization. Increasing the concentration of the weakly correlated component A leads to a significant increasing of the quasiparticle weight Z^{B} for both setups. This

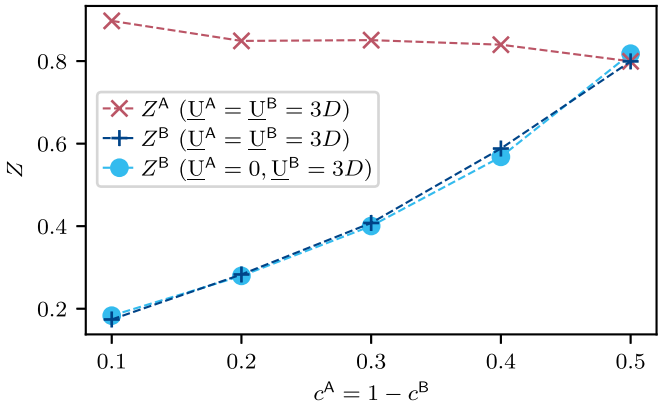

FIG. 4. Quasiparticle weight Z corresponding to $\underline{T}^{AB} = 5.0$ in Figs. 2 and 3 for parameters $\underline{v}^{A} = -\underline{U}^{A}/2$, $\underline{v}^{B} = -\underline{U}^{B}/2$, $\underline{T}^{AA} = \underline{T}^{BB} = 1$, and $\underline{T}^{AB} = 5.0$ at $T = 0$, calculated for a shift $\eta = 0.12$.

can be explained by the increasing number of A-B bonds, which leads to increased mobility of the hopping due to the large value of $\underline{T}^{AB} = 5.0$ compared to the intercomponent hoppings $\underline{T}^{AA} = \underline{T}^{BB} = 1$.

D. Combined effect of diagonal and off-diagonal disorder

In the following, we explore the combined effect of both diagonal and off-diagonal disorder, and their interplay with interaction. We choose a uniform interaction strength $\underline{U}^{A} = \underline{U}^{B} = U$ and introduce diagonal disorder with on-site potentials $\underline{v}^{A} = -1.5D - U/2$, $\underline{v}^{B} = +1.5D - U/2$. This means that the scattering strength is of the magnitude $\delta = (\underline{v}^{B} - \underline{v}^{A})/D = 3$. We consider components with equal bandwidth $\underline{T}^{AA} = \underline{T}^{BB} = 1$ and equal concentration $c^{A} = c^{B} = 0.5$. Thus, the components are particle-hole conjugate and fulfill the relation

$$\underline{\mathbf{g}}^{AA}_{\mathrm{loc}}(z) = -\left[\underline{\mathbf{g}}^{BB}_{\mathrm{loc}}(z)\right]^{*}. \tag{50}$$

Figure 5 shows the average spectral function as well as that for the individual components for different values of the Hubbard parameter U and dimensionless intercomponent hopping amplitudes $\underline{T}^{AB}$. In the case $U = 0$ (first column of Fig. 5) one starts from the split-band limit.

We first investigate the CPA limit $\underline{T}^{AB} = 1$ (second row of Fig. 5). In the split-band limit, there are no correlation effects: One component is basically filled ($n^{A}_{\sigma} \approx 1$), and the other is depleted ($n^{B}_{\sigma} \approx 0$). However, the Hartree energy, $\Sigma^{H}_{\sigma} = n_{\sigma} U$, decreases the effective disorder strength:

$$\begin{aligned}\delta_{\mathrm{eff}} &= \frac{\left(\underline{v}^{B} + n^{B}_{\sigma} U\right) - \left(\underline{v}^{A} + n^{A}_{\sigma} U\right)}{D} \\ &\approx [\underline{v}^{B} - \underline{v}^{A} - U]/D = \delta - U/D.\end{aligned} \tag{51}$$

Switching on the interaction U effectively decreases the scattering strength δ. From $U \approx 2D$ on, the split-band limit at large scattering strength no longer applies; i.e., there is a combination of disorder and interaction effects. For $U = 4D$, we see the upper and lower Hubbard bands for each component, as well as a quasiparticle peak at the Fermi level. For even larger interaction strength ($U = 6D$) a Mott insulating phase is observed. Thus, by increasing U it is possible to tune the system from an alloy-band insulator, through a metallic phase, to a Mott insulating state. Similar results were reported by Lombardo *et al.* [41] for diagonal disorder using CPA+DMFT for somewhat different parameters and a finite-temperature impurity solver.

The behavior obtained in the CPA limit can now be modified by varying $\underline{T}^{AB}$. At $U = 2D$ an off-diagonal hopping $\underline{T}^{AB} < 1$ leads to metallic behavior, while $\underline{T}^{AB} > 1$ favors a band gap. On the other hand, for $U = 6D$ a large $\underline{T}^{AB}$ favors metallicity. For $\underline{T}^{AB} \leqslant 1$ the spectral function is gapped—similar to the result obtained in the Hubbard-I approximation [61].

IV. SUMMARY

We presented a methodological framework for the study of interacting electrons in the presence of diagonal and off-diagonal disorder. The formalism allows one to explore a multicomponent system of electrons with random on-site

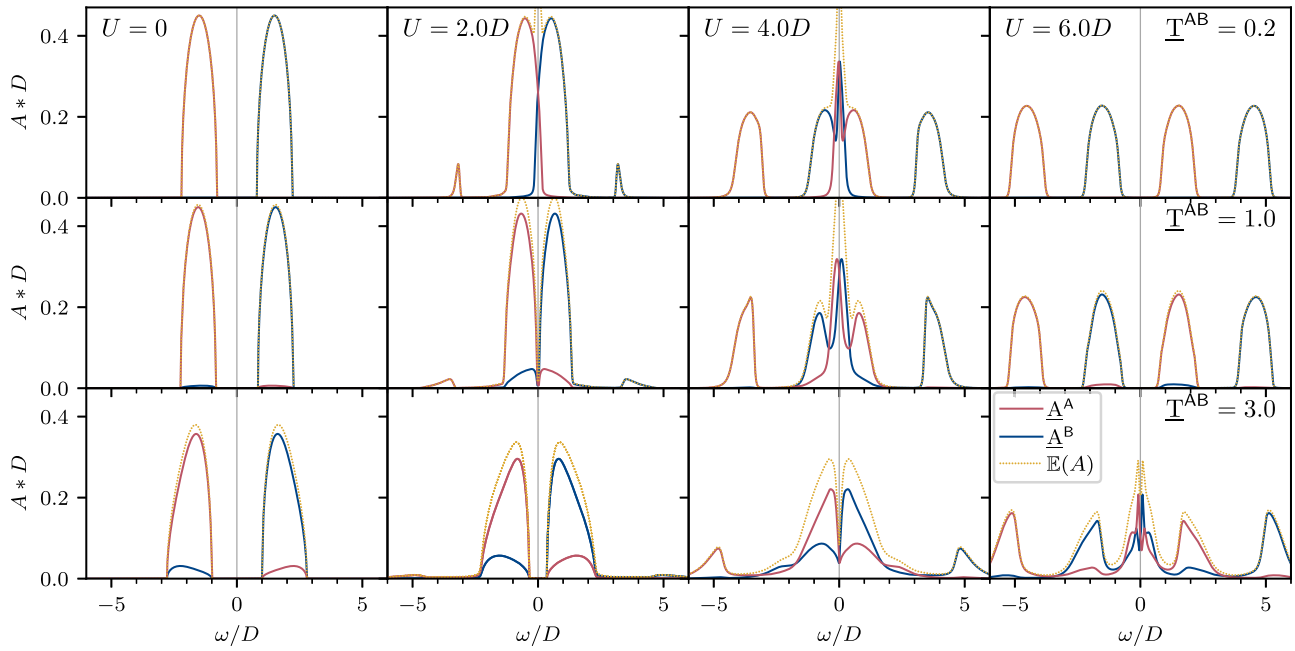

FIG. 5. Comparison of the spectral functions for $\underline{\mathrm{U}}^{\mathrm{A}} = \underline{\mathrm{U}}^{\mathrm{B}} = U$, $-(\underline{\mathrm{v}}^{\mathrm{A}} + U/2) = \underline{\mathrm{v}}^{\mathrm{B}} + U/2 = 1.5D$, $c^{\mathrm{A}} = 0.5 = c^{\mathrm{B}}$, $\underline{\mathrm{T}}^{\mathrm{AA}} = \underline{\mathrm{T}}^{\mathrm{BB}} = 1$, and $T = 0$ for different values of $\underline{\mathrm{T}}^{\mathrm{AB}}$ and U.

interactions and/or potentials as well as random hopping amplitudes. For this purpose the Blackman-Esterling-Berk (BEB) formalism for averaging over off-diagonal disorder was combined with the dynamical mean-field theory (DMFT). We introduced a tensor notation inspired by Koepernik *et al.* [37,38], by which the randomness of the components is transferred to local indicator tensors defined in an extended space. In this representation, the problem can be solved in a single-site approximation, analogous to the coherent potential approximation (CPA). The computational procedure, including the twofold self-consistency and the impurity solver [39], were discussed in detail.

In the limit of zero intercomponent hopping an analytic solution for the BEB approximation of the noninteracting Bethe lattice with the general coordination Z was provided. We established the exact bounds of the spectral function, and showed that these lie within the maximal bound given by the Gershgorin circle theorem [59].

The first application of the BEB+DMFT formalism in tensor formulation was the computation of spectral functions. In particular, we discussed the changes in the spectral function for increasing dimensionless hopping amplitude $\underline{\mathrm{T}}^{\mathrm{AB}}$ and interaction strengths U. For alloy components with the same local interaction, we found a pseudogap in the spectral function of the alloy component with lower concentration. For larger values of $\underline{\mathrm{T}}^{\mathrm{AB}}$ this is accompanied by quasiparticles of the dominant alloy component. The pseudogap and the quasiparticle character were inferred by analyzing the respective self-energies. We found a rather similar behavior in the case of alloy components with different interaction strengths. For the discussion of both diagonal and off-diagonal disorder we studied equal alloy concentrations and equal alloy component bandwidths for a rather large scattering strength $\delta = 3D$. Increasing U while keeping $\underline{\mathrm{T}}^{\mathrm{AB}} \leqslant 1.0$ fixed, the electronic system was found to undergo two transitions: One from the noncorrelated alloy insulator to a metallic state, and then from the metal to a correlated (Mott) insulator. For larger values of $\underline{\mathrm{T}}^{\mathrm{AB}}$ the formation of quasiparticles signals the appearance of a metallic state, which eventually disappears again within the Mott insulating phase for large enough values of U.

Finally, we note that at the CPA+DMFT level our results are in agreement with previous model-Hamiltonian-based publications. As a matter of fact the BEB formulation is applicable to band-structure schemes [37,38,44] also for nonorthogonal basis sets. The present formulation can be naturally extended following the CPA+DMFT [62] methodology with similar computational costs. Work along this line is in progress.

ACKNOWLEDGMENTS

Financial support by the Deutsche Forschungsgemeinschaft through TRR80 (project F6) Project No. 107745057 is gratefully acknowledged. Y.Z. is supported in part by the NSF China Grant No. 12004383 and the Fundamental Research Funds for the Central Universities. H.T. gratefully acknowledges support from NSF Grants No. OAC-1931367 and No. DMR-1944974 grants. K.M.T. is partially supported by NSF Grants No. DMR-1728457 and No. OAC-1931445 grants.

APPENDIX A: AN EXPLICIT EXAMPLE OF THE EXTENDED HAMILTONIAN MATRIX

Here we provide an explicit example of the Hamiltonian matrix $\boldsymbol{H}$ and the extended Hamiltonian $\underline{\mathbf{H}}$. We consider a small system—a chain with three sites $(1, 2, 3)$ and two

components A and B. For this chain the Hamiltonian matrix reads

$$\boldsymbol{H} = \begin{pmatrix} v_1 & t_{12} & t_{13} \\ t_{21} & v_2 & t_{23} \\ t_{31} & t_{32} & v_3 \end{pmatrix} - \mathbb{1}\mu. \tag{A1}$$

This is a random matrix since it depends on the configuration. We consider $c^{\mathsf{A}} = 1/3$ and $c^{\mathsf{B}} = 2/3$; then one possible configuration is A-B-B. According to Eq. (8), the Hamiltonian matrix of this configuration takes the values

$$\boldsymbol{H}_{\mathsf{ABB}} = \begin{pmatrix} \underline{v}^{\mathsf{A}} & \underline{t}^{\mathsf{AB}}(a) & \underline{t}^{\mathsf{AB}}(2a) \\ \underline{t}^{\mathsf{BA}}(a) & \underline{v}^{\mathsf{B}} & \underline{t}^{\mathsf{BB}}(a) \\ \underline{t}^{\mathsf{BA}}(2a) & \underline{t}^{\mathsf{BB}}(a) & \underline{v}^{\mathsf{B}} \end{pmatrix} - \mathbb{1}\mu, \tag{A2}$$

where a is the distance between neighboring sites. By contrast, the extended Hamiltonian matrix $\underline{\mathbf{H}}$ does not depend on the specific configuration. We can choose a matrix representation of the tensor $\underline{\mathbf{H}}$ shown in Eq. (12), by grouping the legs i and α on the same side. This is done explicitly defining the combined index $n = (i, \alpha)$ [$m = (j, \beta)$]. We count $n = 2i - 1 + n_\alpha$ with $n_{\mathsf{A}} = 0$ and $n_{\mathsf{B}} = 1$. Then the extended Hamiltonian $\underline{\mathrm{H}}^{\alpha\beta}_{ij} = \underline{\mathrm{H}}_{nm}$ reads

$$\underline{\mathbf{H}} = \begin{pmatrix} \underline{\mathbf{v}}^{\mathrm{A}} & 0 & \underline{\mathbf{t}}^{\mathrm{AA}}(a) & \underline{\mathbf{t}}^{\mathrm{AB}}(a) & \underline{\mathbf{t}}^{\mathrm{AA}}(2a) & \underline{\mathbf{t}}^{\mathrm{AB}}(2a) \\ 0 & \underline{\mathbf{v}}^{\mathrm{B}} & \underline{\mathbf{t}}^{\mathrm{BA}}(a) & \underline{\mathbf{t}}^{\mathrm{BB}}(a) & \underline{\mathbf{t}}^{\mathrm{BA}}(2a) & \underline{\mathbf{t}}^{\mathrm{BB}}(2a) \\ \underline{\mathbf{t}}^{\mathrm{AA}}(a) & \underline{\mathbf{t}}^{\mathrm{AB}}(a) & \underline{\mathbf{v}}^{\mathrm{A}} & 0 & \underline{\mathbf{t}}^{\mathrm{AA}}(a) & \underline{\mathbf{t}}^{\mathrm{AB}}(a) \\ \underline{\mathbf{t}}^{\mathrm{BA}}(a) & \underline{\mathbf{t}}^{\mathrm{BB}}(a) & 0 & \underline{\mathbf{v}}^{\mathrm{B}} & \underline{\mathbf{t}}^{\mathrm{BA}}(a) & \underline{\mathbf{t}}^{\mathrm{BB}}(a) \\ \underline{\mathbf{t}}^{\mathrm{AA}}(2a) & \underline{\mathbf{t}}^{\mathrm{AB}}(2a) & \underline{\mathbf{t}}^{\mathrm{AA}}(a) & \underline{\mathbf{t}}^{\mathrm{AB}}(a) & \underline{\mathbf{v}}^{\mathrm{A}} & 0 \\ \underline{\mathbf{t}}^{\mathrm{BA}}(2a) & \underline{\mathbf{t}}^{\mathrm{BB}}(2a) & \underline{\mathbf{t}}^{\mathrm{BA}}(a) & \underline{\mathbf{t}}^{\mathrm{BB}}(a) & 0 & \underline{\mathbf{v}}^{\mathrm{B}} \end{pmatrix} - \mathbb{1}\mu. \tag{A3}$$

This $MN \times MN = 6 \times 6$ matrix contains all M^N possible configurations for the $N = 3$ site problem with $M = 2$ components and is independent of the concentrations c^α. A specific configuration can be selected by applying an appropriate indicator tensor $\underline{\boldsymbol{\eta}}$. For the configuration A-B-B, $\underline{\eta}^{\alpha}_{ij} = \underline{\eta}_{nj}$ takes the form

$$\underline{\boldsymbol{\eta}}^{\mathsf{T}}_{\mathsf{ABB}} = \begin{pmatrix} 1 & 0 & 0 & 0 & 0 & 0 \\ 0 & 0 & 0 & 1 & 0 & 0 \\ 0 & 0 & 0 & 0 & 0 & 1 \end{pmatrix}, \tag{A4}$$

and we obtain the Hamiltonian matrix for this configuration from

$$\boldsymbol{H}_{\mathsf{ABB}} = \underline{\boldsymbol{\eta}}^{\mathsf{T}}_{\mathsf{ABB}} \underline{\mathbf{H}} \underline{\boldsymbol{\eta}}_{\mathsf{ABB}}. \tag{A5}$$

While the matrix representation is suitable for performing calculations, the tensor notation is often clearer. The elements diagonal in components α of the extended Hamiltonian read

$$\underline{\mathbf{H}}^{\alpha\alpha} = \begin{pmatrix} \underline{\mathrm{v}}^{\alpha} & \underline{\mathrm{t}}^{\alpha\alpha}(a) & \underline{\mathrm{t}}^{\alpha\alpha}(2a) \\ \underline{\mathrm{t}}^{\alpha\alpha}(a) & \underline{\mathrm{v}}^{\alpha} & \underline{\mathrm{t}}^{\alpha\alpha}(a) \\ \underline{\mathrm{t}}^{\alpha\alpha}(2a) & \underline{\mathrm{t}}^{\alpha\alpha}(a) & \underline{\mathrm{v}}^{\alpha} \end{pmatrix} - \mathbb{1}\mu, \tag{A6}$$

the off-diagonal elements $\alpha \neq \beta$ read

$$\underline{\mathbf{H}}^{\alpha\beta} = \begin{pmatrix} 0 & \underline{\mathrm{t}}^{\alpha\beta}(a) & \underline{\mathrm{t}}^{\alpha\beta}(2a) \\ \underline{\mathrm{t}}^{\alpha\beta}(a) & 0 & \underline{\mathrm{t}}^{\alpha\beta}(a) \\ \underline{\mathrm{t}}^{\alpha\beta}(2a) & \underline{\mathrm{t}}^{\alpha\beta}(a) & 0 \end{pmatrix}, \tag{A7}$$

and the indicator tensor for the configuration A-B-B is given by the elements

$$\underline{\boldsymbol{\eta}}^{\mathsf{A}}_{\mathsf{ABB}} = \begin{pmatrix} 1 & 0 & 0 \\ 0 & 0 & 0 \\ 0 & 0 & 0 \end{pmatrix} \quad \text{and} \quad \underline{\boldsymbol{\eta}}^{\mathsf{B}}_{\mathsf{ABB}} = \begin{pmatrix} 0 & 0 & 0 \\ 0 & 1 & 0 \\ 0 & 0 & 1 \end{pmatrix}. \tag{A8}$$

APPENDIX B: EFFICIENT EVALUATION OF THE LOCAL GREEN'S FUNCTION AND ITS INVERSE

To solve the BEB self-consistency equation, we need to repeatedly evaluate the effective local Green's function

$$\underline{\mathbf{g}}_{\mathrm{loc}}(z) = \frac{1}{N} \sum_k [\underline{\boldsymbol{\xi}}(z) - \underline{\mathbf{T}}\epsilon_k]^{-1}, \tag{B1}$$

with $\underline{\boldsymbol{\xi}}(z) = \mathbb{1}z - \underline{\mathbf{S}}(z)$, or rather its inverse $(\underline{\mathbf{g}}_{\mathrm{loc}})^{-1}$. A naive evaluation would be computationally costly, since one needs to invert a matrix for every k point and every frequency point. While this is feasible for small matrices, it has the potential risk of inaccurate k summations (or integrations), especially for a DOS with singularities as for a one-dimensional or square lattice. Therefore, we employ an algorithm based on the *compact* singular value decomposition (SVD) of the matrix $\underline{\mathbf{T}}$,

$$\underline{\mathbf{T}} = \boldsymbol{U}\boldsymbol{\sigma}\boldsymbol{V}^\dagger = \boldsymbol{U}\boldsymbol{\sigma}^{1/2}\boldsymbol{\sigma}^{1/2}\boldsymbol{V}^\dagger =: \tilde{\boldsymbol{U}}\tilde{\boldsymbol{V}}^\dagger, \tag{B2}$$

which we use to split the matrix; here we partitioned the singular values symmetrically as $\tilde{\boldsymbol{U}} = \boldsymbol{U}\boldsymbol{\sigma}^{1/2}$, $\tilde{\boldsymbol{V}}^\dagger = \sigma^{1/2}\boldsymbol{V}^\dagger$. It is important to use the compact SVD as we will explicitly use the inverse $\boldsymbol{\sigma}^{-1}$. Numerically, the need to truncate small singular values arises. We note that for the binary alloy the rank-1 case, where the SVD has to be truncated, is given for a hopping matrix of the type

$$\begin{pmatrix} \underline{\mathrm{T}}^{\mathsf{AA}} & \sqrt{\underline{\mathrm{T}}^{\mathsf{AA}}\underline{\mathrm{T}}^{\mathsf{BB}}} \\ \sqrt{\underline{\mathrm{T}}^{\mathsf{AA}}\underline{\mathrm{T}}^{\mathsf{BB}}} & \underline{\mathrm{T}}^{\mathsf{BB}} \end{pmatrix} = \begin{pmatrix} \sqrt{\underline{\mathrm{T}}^{\mathsf{AA}}} \\ \sqrt{\underline{\mathrm{T}}^{\mathsf{BB}}} \end{pmatrix} \begin{pmatrix} \sqrt{\underline{\mathrm{T}}^{\mathsf{AA}}} & \sqrt{\underline{\mathrm{T}}^{\mathsf{BB}}} \end{pmatrix}. \tag{B3}$$

This is the structure of the hopping matrix discussed by Shiba [63]. Another prominent rank-1 example is the CPA limit with $\underline{\mathrm{T}}^{\mathsf{AA}} = \underline{\mathrm{T}}^{\mathsf{AB}} = \underline{\mathrm{T}}^{\mathsf{BB}} = 1$.

The matrix inverse $[\underline{\boldsymbol{\xi}}(z) - \underline{\mathbf{T}}\epsilon_k]^{-1}$ is calculated using the Woodbury matrix identity [64]. Furthermore, we calculate the

eigendecomposition

$$\tilde{\boldsymbol{V}}^\dagger \underline{\boldsymbol{\xi}}^{-1}(z)\tilde{\boldsymbol{U}} = \boldsymbol{P}(z)\boldsymbol{d}(z)\boldsymbol{P}^{-1}(z), \tag{B4}$$

where $\boldsymbol{d}(z)$ is the diagonal matrix of eigenvalues. The k-dependent Green's function can be expressed as

$$\underline{\mathbf{G}}(z,k) = \underline{\boldsymbol{\xi}}^{-1} - \underline{\boldsymbol{\xi}}^{-1}\tilde{\boldsymbol{U}}\boldsymbol{P}\left[\boldsymbol{d} - \frac{\mathbb{1}}{\epsilon_k}\right]^{-1}\boldsymbol{P}^{-1}\tilde{\boldsymbol{V}}^\dagger\underline{\boldsymbol{\xi}}^{-1}, \tag{B5}$$

where we did not write the z dependence explicitly. We note that only the term in the square brackets depends on k. Since it contains only diagonal matrices, the matrix inverse only involves the reciprocal matrix elements. We look at a particular diagonal element with the z-dependent eigenvalue $\boldsymbol{d}_{ii}(z) = \lambda_i(z)$,

$$-\left[\lambda_i(z) - \frac{1}{\epsilon_k}\right]^{-1} = \frac{1}{1/\lambda_i(z) - \epsilon_k}\frac{1}{\lambda_i^2(z)} - \frac{1}{\lambda_i(z)}. \tag{B6}$$

It is straightforward to perform the k summation, as we have the standard form of the lattice Hilbert transform,

$$\frac{1}{N}\sum_k \frac{1}{z-\epsilon_k} =: g_0(z), \tag{B7}$$

evaluated at $1/\lambda_i$. For simple lattices like the Bethe lattice we know the analytic expression for g_0; a numerical integration can then be avoided. For the local Green's function we obtain the lengthy expression

$$\underline{\mathbf{g}}_{\text{loc}} = \underline{\boldsymbol{\xi}}^{-1} + \underline{\boldsymbol{\xi}}^{-1}\tilde{\boldsymbol{U}}\boldsymbol{P}[\boldsymbol{d}^{-1}g_0(\boldsymbol{d}^{-1}) - \mathbb{1}]\boldsymbol{d}^{-1}\boldsymbol{P}^{-1}\tilde{\boldsymbol{V}}^\dagger\underline{\boldsymbol{\xi}}^{-1}, \tag{B8}$$

where again the z dependence was not written out. For the self-consistency equation of the BEB formalism one only needs the inverse of $\underline{\mathbf{g}}_{\text{loc}}$. The Woodbury matrix identity yields the simpler expression

$$\underline{\mathbf{g}}_{\text{loc}}^{-1}(z) = \underline{\boldsymbol{\xi}}(z) + \tilde{\boldsymbol{U}}\boldsymbol{P}(z)\left[\frac{1}{g_0(1/\boldsymbol{d}(z))} - 1/\boldsymbol{d}(z)\right]\boldsymbol{P}^{-1}(z)\tilde{\boldsymbol{V}}^\dagger, \tag{B9}$$

where we explicitly noted the inverse of the diagonal matrices by reciprocal matrix elements.

Considering that the main cost of a naive evaluation of $\underline{\mathbf{g}}_{\text{loc}}^{-1}$ arises from the matrix inversion, this amounts to $N_z(N_k+1)$ matrix inversions, where N_z is the number of frequency points and N_k is the number of k points required for the integration. The alternative algorithm proposed here requires, on the other hand, N_z matrix inversions due to the calculation of $\underline{\boldsymbol{\xi}}^{-1}(z)$, and another N_z matrix diagonalizations in the compact space of the SVD. In practice, the calculations were well behaved, and we encountered no numerical problems regarding the diagonalization of Eq. (B4).

For the common case of full rank $\underline{\mathbf{T}}$, we can use the unitarity $\boldsymbol{U}^\dagger = \boldsymbol{U}^{-1}$ and $\boldsymbol{V}^\dagger = \boldsymbol{V}^{-1}$ to simplify the formulas further. We obtain the simple formulas for the local Green's function,

$$\underline{\mathbf{g}}_{\text{loc}}(z) = \boldsymbol{V}\boldsymbol{\sigma}^{-1/2}\boldsymbol{P}(z)g_0(1/\boldsymbol{d}(z))\boldsymbol{P}^{-1}(z)\boldsymbol{\sigma}^{-1/2}\boldsymbol{U}^\dagger, \tag{B10}$$

and its inverse,

$$\underline{\mathbf{g}}_{\text{loc}}^{-1}(z) = \tilde{\boldsymbol{U}}\boldsymbol{P}(z)\frac{1}{g_0(1/\boldsymbol{d}(z))}\boldsymbol{P}^{-1}(z)\tilde{\boldsymbol{V}}^\dagger. \tag{B11}$$

Furthermore, we can directly calculate the matrix diagonalization of

$$\boldsymbol{\sigma}^{-1/2}\boldsymbol{U}^\dagger\underline{\boldsymbol{\xi}}(z)\boldsymbol{V}\boldsymbol{\sigma}^{-1/2} = \boldsymbol{P}(z)\boldsymbol{d}^{-1}(z)\boldsymbol{P}^{-1}(z), \tag{B12}$$

avoiding the need for the N_z matrix inversions for $\underline{\boldsymbol{\xi}}(z)$.

APPENDIX C: BEB SELF-CONSISTENCY EQUATION WITH RENORMALIZED INDICATOR TENSORS

For $\alpha \neq \beta$, the high-frequency expansion of the effective medium yields

$$\underline{\mathrm{S}}^{\alpha\beta}(z) = -\epsilon_{(1)}\underline{\mathrm{T}}^{\alpha\beta} + \mathcal{O}(z^{-1}), \tag{C1}$$

$$\underline{\mathrm{S}}^{\alpha\alpha}(z) = \frac{c^\alpha - 1}{c^\alpha}z + \frac{\underline{\mathrm{v}}^\alpha - \mu + \bar{c}^\alpha\underline{\mathrm{T}}^{\alpha\alpha}\epsilon_{(1)}}{c^\alpha} + \mathcal{O}(z^{-1}), \tag{C2}$$

where $\epsilon_{(1)} = \int d\epsilon\,\rho(\epsilon)\epsilon$ is the first moment of the DOS, which vanishes for lattices with a symmetric DOS, $\underline{\mathrm{v}}$ incorporates the static part of the self-energy $\Sigma^\alpha(z)$, and $\bar{c}^\alpha = 1 - c^\alpha$ is the concentration complement. The diagonal of the effective medium, $\underline{\mathrm{S}}^{\alpha\alpha}(z)$, has a contribution which grows linearly in z, and the on-site energies are multiplied by the inverse of the concentration. The origin of this peculiar structure is evident from Eq. (17) and the definition in Eq. (20). Unlike the diagonal elements of a one-particle Green's function which behave like $1/z$ for large z, the effective local Green's function $\underline{\mathbf{g}}_{\text{loc}}(z)$ behaves like $\boldsymbol{c}/z$. The definition in terms of the effective medium, however, has the regular form of $[\mathbb{1}z + \cdots]^{-1}$. This can be resolved by introducing a renormalized version of the component space. Instead of the indicator tensor $\underline{\boldsymbol{\eta}}$, Eq. (10), we use the concentration-scaled indicator tensor

$$\underline{\gamma}^\alpha_{ij} = \sqrt{c^\alpha}\mathbb{1}_{\mathbb{S}^\alpha}(i)\delta_{ij} \tag{C3}$$

and the Moore-Penrose inverse [65,66] $\underline{\boldsymbol{\gamma}}^+$ (which is in this case the left inverse, i.e., $\underline{\boldsymbol{\gamma}}^+\underline{\boldsymbol{\gamma}} = \mathbb{1}$) of its equivalent matrix representation. The components of the Moore-Penrose inverse read

$$\underline{\gamma}^{+\,\alpha}_{\ \ ij} = \begin{cases} \frac{1}{\sqrt{c^\alpha}}\mathbb{1}_{\mathbb{S}^\alpha}(i)\delta_{ij} & \text{if} \quad c^\alpha > 0 \\ 0 & \text{if} \quad c^\alpha = 0. \end{cases} \tag{C4}$$

We can express the projector in Eq. (13) with the $\underline{\boldsymbol{\gamma}}$ tensor:

$$\underline{\boldsymbol{\chi}} = \underline{\boldsymbol{\gamma}}\underline{\boldsymbol{\gamma}}^+. \tag{C5}$$

For the renormalized BEB formalism, we define the component Green's function and the Hamiltonian matrix in terms of $\underline{\boldsymbol{\gamma}}$ and the inverse $\underline{\boldsymbol{\gamma}}^+$ as

$$\underline{\tilde{\mathbf{G}}}(z) \coloneqq (\underline{\boldsymbol{\gamma}}^+)^\intercal\boldsymbol{G}(z)\underline{\boldsymbol{\gamma}}^+, \quad \boldsymbol{H} =: \underline{\boldsymbol{\gamma}}\underline{\tilde{\mathbf{H}}}\underline{\boldsymbol{\gamma}}^\intercal. \tag{C6}$$

Compared to the definitions in Sec. II B, the Green's function and the Hamiltonian are scaled by the concentration. This can be conveniently demonstrated in the locator expansion

$$\boldsymbol{G}(z) = \boldsymbol{g}(z) + \boldsymbol{g}(z)\boldsymbol{T}\boldsymbol{G}(z), \tag{C7}$$

where $\boldsymbol{g}(z) = [\mathbb{1}z - \boldsymbol{v}]^{-1}$ is the locator and $(\boldsymbol{T})_{ij} = t_{ij}$. Sandwiching this equation by $(\underline{\boldsymbol{\gamma}}^+)^\intercal$ and $\underline{\boldsymbol{\gamma}}^+$, we obtain

$$(\underline{\boldsymbol{\gamma}}^+)^\intercal\boldsymbol{G}(z)\underline{\boldsymbol{\gamma}}^+ = (\underline{\boldsymbol{\gamma}}^+)^\intercal\boldsymbol{g}(z)\underline{\boldsymbol{\gamma}}^+ + (\underline{\boldsymbol{\gamma}}^+)^\intercal\boldsymbol{g}(z)\underline{\boldsymbol{\gamma}}^+\underline{\boldsymbol{\gamma}}\boldsymbol{T}\underline{\boldsymbol{\gamma}}^\intercal(\underline{\boldsymbol{\gamma}}^+)^\intercal\boldsymbol{G}(z)\underline{\boldsymbol{\gamma}}^+, \tag{C8}$$

where we inserted the identity $\underline{\boldsymbol{\gamma}}^{+}\underline{\boldsymbol{\gamma}} = \mathbb{1}$. This can be written in terms of the renormalized component quantities

$$\underline{\tilde{\mathbf{G}}}(z) = \underline{\tilde{\mathbf{g}}}(z) + \underline{\tilde{\mathbf{g}}}(z)\underline{\tilde{\mathbf{T}}}\,\underline{\tilde{\mathbf{G}}}(z). \tag{C9}$$

Compared to the regular BEB formalism the Green's functions are scaled with the reciprocal concentration, and the hopping matrix with the concentration $\underline{\tilde{T}}_{ij}^{\alpha\beta} = \sqrt{c^{\alpha}}\underline{t}^{\alpha\beta}(|\mathbf{r}_i - \mathbf{r}_j|)\sqrt{c^{\beta}}$. The renormalized component Green's function relates now to the one-particle Green's function in the following way:

$$\mathbb{E}\big(\tilde{\mathrm{G}}_{ij}^{\alpha\beta}\big) = \begin{cases} \mathbb{E}(G_{ii}(z)|i \mapsto \alpha)\delta^{\alpha\beta} & \text{if} \quad i = j \\ \sqrt{c^{\alpha}c^{\beta}}\,\mathbb{E}(G_{ii}(z)|i, j \mapsto \alpha, \beta) & \text{if} \quad i \neq j. \end{cases} \tag{C10}$$

There is no more concentration prefactor for the local Green's function, which is the central quantity of the BEB formalism, since it is a local theory. The renormalized version of the self-consistency equation, Eqs. (25) and (26), reads

$$0 = \underline{\tilde{\mathbf{g}}}_{\mathrm{loc}}^{-1}(z) - \underline{\bar{\tilde{\mathbf{g}}}}^{-1}(z), \tag{C11}$$

with the diagonal matrix

$$\underline{\bar{\tilde{\mathrm{g}}}}^{\alpha\beta}(z) = \frac{c^{\alpha}\delta^{\alpha\beta}}{\big(\underline{\tilde{\mathbf{g}}}_{\mathrm{loc}}^{-1}\big)^{\alpha\alpha} + \underline{\tilde{\mathrm{S}}}^{\alpha\alpha} - \bar{c}^{\alpha}z + c^{\alpha}(\mu - \underline{\mathrm{v}}^{\alpha} - \Sigma^{\alpha})}. \tag{C12}$$

With $\alpha \neq \beta$, the high-frequency expansion of the renormalized effective medium yields

$$\underline{\tilde{\mathrm{S}}}^{\alpha\beta}(z) = -\epsilon_{(1)}\sqrt{c^{\alpha}}\underline{\mathrm{T}}^{\alpha\beta}\sqrt{c^{\beta}} + \mathcal{O}(z^{-1}), \tag{C13}$$

$$\underline{\tilde{\mathrm{S}}}^{\alpha\alpha}(z) = \underline{\mathrm{v}}^{\alpha} - \mu + \bar{c}^{\alpha}\underline{\mathrm{T}}^{\alpha\alpha}\epsilon_{(1)} + \mathcal{O}(z^{-1}). \tag{C14}$$

The scaling removes the contribution proportional to z, and for a symmetric DOS the static part is simply the on-site energy of the components. Furthermore, the static part remains finite with vanishing concentration.

APPENDIX D: HYBRIDIZATION OF THE BETHE LATTICE

Specific to the BEB+DMFT scheme is an alloy-component-dependent hybridization function $\Delta^{\alpha}(z)$ computed according to Eq. (28). The hybridization function describes the hopping process into and out of the impurity site. The special form of the lattice Hilbert transform $g_0(z)$ for the Bethe lattice,

$$z - 1/g_0(z) = (D/2)^2 g_0(z), \tag{D1}$$

gives a direct relation between the hybridization function $\Delta^{\alpha}(z)$ and the effective local Green's function $\underline{\mathbf{g}}_{\mathrm{loc}}(z)$ [Eq. (20)]. We promote the hybridization function in Eq. (28) to a full hybridization matrix

$$\underline{\boldsymbol{\Delta}}(z) = \mathbb{1}z - \underline{\mathbf{S}}(z) - \underline{\mathbf{g}}_{\mathrm{loc}}^{-1}(z) =: \underline{\boldsymbol{\xi}}(z) - \underline{\mathbf{g}}_{\mathrm{loc}}^{-1}(z), \tag{D2}$$

whose diagonal elements are the physical hybridization function $\underline{\Delta}^{\alpha\alpha} = \Delta^{\alpha}$. Using the representation in Eq. (B9) given in section B, we can apply the identity from Eq. (D1):

$$\underline{\boldsymbol{\Delta}}(z) = (D/2)^2\tilde{\boldsymbol{U}}\boldsymbol{P}(z)g_0\big(1/\boldsymbol{d}(z)\big)\boldsymbol{P}^{-1}(z)\tilde{\boldsymbol{V}}^{\dagger}. \tag{D3}$$

Likewise, the matrix $\underline{\mathbf{T}}\underline{\mathbf{g}}_{\mathrm{loc}}(z)\underline{\mathbf{T}}$ can be expressed using Eqs. (B2), (B4), and (B8):

$$\underline{\mathbf{T}}\underline{\mathbf{g}}_{\mathrm{loc}}(z)\underline{\mathbf{T}} = \tilde{\boldsymbol{U}}\boldsymbol{P}(z)g_0\big(1/\boldsymbol{d}(z)\big)\boldsymbol{P}^{-1}(z)\tilde{\boldsymbol{V}}^{\dagger}. \tag{D4}$$

Thus, comparing Eqs. (D3) and (D4), we identify the relation for the Bethe lattice:

$$\underline{\boldsymbol{\Delta}}(z) = (D/2)^2\underline{\mathbf{T}}\underline{\mathbf{g}}_{\mathrm{loc}}(z)\underline{\mathbf{T}}. \tag{D5}$$

The diagonal elements are the hybridization function, which reads

$$\Delta^{\alpha}(z) = (D/2)^2\sum_{\beta}|\underline{\mathrm{T}}^{\alpha\beta}|^2\underline{\mathbf{g}}_{\mathrm{loc}}^{\beta\beta}(z). \tag{D6}$$

In the CPA case, $\underline{\mathrm{T}}^{\alpha\beta} = 1$, we evidently recover the component-independent hybridization:

$$\Delta^{\alpha}(z) = (D/2)^2\sum_{\alpha}\underline{\mathbf{g}}_{\mathrm{loc}}^{\alpha\alpha}(z) = (D/2)^2\mathbb{E}(G(z)). \tag{D7}$$

For the case of a binary alloy shown by Fig. 5, we see that for $\underline{\mathrm{T}}^{\mathsf{AB}} < 1 = \underline{\mathrm{T}}^{\alpha\alpha}$ the hybridization for A stems mostly from A sites, while for $\underline{\mathrm{T}}^{\mathsf{AB}} > 1 = \underline{\mathrm{T}}^{\alpha\alpha}$ the main contribution to the hybridization of A comes from the B sites.

[1] P. A. Lee and T. V. Ramakrishnan, Rev. Mod. Phys. **57**, 287 (1985).
[2] N. F. Mott, *Metal-Insulator Transitions*, 2nd ed. (Taylor & Francis, London, 1990).
[3] D. Belitz and T. R. Kirkpatrick, Rev. Mod. Phys. **66**, 261 (1994).
[4] N. F. Mott, Proc. Phys. Soc. A **62**, 416 (1949).
[5] M. Imada, A. Fujimori, and Y. Tokura, Rev. Mod. Phys. **70**, 1039 (1998).
[6] P. W. Anderson, Phys. Rev. **109**, 1492 (1958).
[7] F. Evers and A. D. Mirlin, Rev. Mod. Phys. **80**, 1355 (2008).
[8] *50 Years of Anderson Localization*, edited by E. Abrahams (World Scientific, Singapore, 2010).
[9] E. Abrahams, S. V. Kravchenko, and M. P. Sarachik, Rev. Mod. Phys. **73**, 251 (2001).
[10] *Conductor-Insulator Quantum Phase Transitions*, edited by V. Dobrosavljevic, N. Trivedi, and J. M. Valles, Jr. (Oxford University Press, Oxford, 2012).
[11] R. Nandkishore and D. A. Huse, Annu. Rev. Condens. Matter Phys. **6**, 15 (2015).
[12] D. A. Abanin, E. Altman, I. Bloch, and M. Serbyn, Rev. Mod. Phys. **91**, 021001 (2019).
[13] J. M. Ziman, *Models of Disorder: The Theoretical Physics of Homogeneously Disordered System* (Cambridge University Press, Cambidge, U.K., 1979).

[14] P. Soven, Phys. Rev. **156**, 809 (1967).
[15] D. W. Taylor, Phys. Rev. **156**, 1017 (1967).
[16] B. Velický, S. Kirkpatrick, and H. Ehrenreich, Phys. Rev. **175**, 747 (1968).
[17] R. J. Elliott, J. A. Krumhansl, and P. L. Leath, Rev. Mod. Phys. **46**, 465 (1974).
[18] E. N. Economou, *Green's Functions in Quantum Physics*, Vol. 7 (Springer Science & Business Media, 2006).
[19] A. Gonis, *Green Functions for Ordered and Disordered Systems* (North-Holland, Amsterdam, 1992).
[20] W. Metzner and D. Vollhardt, Phys. Rev. Lett. **62**, 324 (1989).
[21] A. Georges and G. Kotliar, Phys. Rev. B **45**, 6479 (1992).
[22] M. Jarrell, Phys. Rev. Lett. **69**, 168 (1992).
[23] A. Georges, G. Kotliar, W. Krauth, and M. J. Rozenberg, Rev. Mod. Phys. **68**, 13 (1996).
[24] G. Kotliar and D. Vollhardt, Phys. Today **57**, 53 (2004).
[25] R. Vlaming and D. Vollhardt, Phys. Rev. B **45**, 4637 (1992).
[26] V. Janiš and D. Vollhardt, Phys. Rev. B **46**, 15712 (1992).
[27] M. Milovanović, S. Sachdev, and R. N. Bhatt, Phys. Rev. Lett. **63**, 82 (1989).
[28] V. Dobrosavljević and G. Kotliar, Phys. Rev. Lett. **71**, 3218 (1993).
[29] V. Dobrosavljević and G. Kotliar, Phys. Rev. B **50**, 1430 (1994).
[30] M. Ulmke and R. T. Scalettar, Phys. Rev. B **55**, 4149 (1997).
[31] P. J. H. Denteneer, R. T. Scalettar, and N. Trivedi, Phys. Rev. Lett. **87**, 146401 (2001).
[32] E. Miranda and V. Dobrosavljevic, in *Conductor-Insulator Quantum Phase Transitions*, edited by V. Dobrosavljević, N. Trivedi, and J. M. Valles, Jr. (Oxford University Press, Oxford, 2012), p. 161.
[33] J. A. Blackman, D. M. Esterling, and N. F. Berk, Phys. Rev. B **4**, 2412 (1971).
[34] D. M. Esterling, Phys. Rev. B **12**, 1596 (1975).
[35] H. Terletska, C. E. Ekuma, C. Moore, K.-M. Tam, J. Moreno, and M. Jarrell, Phys. Rev. B **90**, 094208 (2014).
[36] Y. Zhang, R. Nelson, E. Siddiqui, K.-M. Tam, U. Yu, T. Berlijn, W. Ku, N. S. Vidhyadhiraja, J. Moreno, and M. Jarrell, Phys. Rev. B **94**, 224208 (2016).
[37] K. Koepernik, B. Velický, R. Hayn, and H. Eschrig, Phys. Rev. B **55**, 5717 (1997).
[38] K. Koepernik, B. Velický, R. Hayn, and H. Eschrig, Phys. Rev. B **58**, 6944 (1998).
[39] D. Bauernfeind, M. Zingl, R. Triebl, M. Aichhorn, and H. G. Evertz, Phys. Rev. X **7**, 031013 (2017).
[40] M. Ulmke, V. Janiš, and D. Vollhardt, Phys. Rev. B **51**, 10411 (1995).
[41] P. Lombardo, R. Hayn, and G. I. Japaridze, Phys. Rev. B **74**, 085116 (2006).
[42] A. Gonis and J. W. Garland, Phys. Rev. B **16**, 1495 (1977).
[43] D. A. Papaconstantopoulos, A. Gonis, and P. M. Laufer, Phys. Rev. B **40**, 12196 (1989).
[44] A. Herbig, R. Heid, and R. Eder, Phys. Rev. B **96**, 205128 (2017).
[45] A. M. Shvaika, Phys. Rev. B **67**, 075101 (2003).
[46] S. Burdin and P. Fulde, Phys. Rev. B **76**, 104425 (2007).
[47] S. Karlin and H. E. Taylor, *A First Course in Stochastic Processes*, 2nd ed. (Academic Press, New York, 1975).
[48] D. Vollhardt, in *Lectures on the Physics of Strongly Correlated Systems XIV*, Vol. 1297, edited by A. Avella and F. Mancini (American Institute of Physics, Melville, NY, 2010), p. 339.
[49] A. Weh and A. Östlin, Derweh/gftools: Gftool 0.9.0 release, 2021, http://doi.org/10.5281/zenodo.4744546.
[50] S. R. White, Phys. Rev. Lett. **69**, 2863 (1992).
[51] U. Schollwöck, Rev. Mod. Phys. **77**, 259 (2005).
[52] J. Haegeman, J. I. Cirac, T. J. Osborne, I. Pižorn, H. Verschelde, and F. Verstraete, Phys. Rev. Lett. **107**, 070601 (2011).
[53] C. Lubich, I. V. Oseledets, and B. Vandereycken, SIAM J. Numer. Anal. **53**, 917 (2015).
[54] J. Haegeman, C. Lubich, I. Oseledets, B. Vandereycken, and F. Verstraete, Phys. Rev. B **94**, 165116 (2016).
[55] D. Bauernfeind and M. Aichhorn, SciPost Phys. **8**, 24 (2020).
[56] R. Bulla, A. C. Hewson, and T. Pruschke, J. Phys.: Condens. Matter **10**, 8365 (1998).
[57] E. Müller-Hartmann, Solid State Commun. **12**, 1269 (1973).
[58] R. Mills and P. Ratanavararaksa, Phys. Rev. B **18**, 5291 (1978).
[59] S. Gershgorin, Izv. Akad. Nauk. USSR Otd. Fiz.-Mat. Nauk **7**, 749 (1931).
[60] K. Byczuk, W. Hofstetter, and D. Vollhardt, Phys. Rev. B **69**, 045112 (2004).
[61] J. Hubbard, Proc. R. Soc. London A **276**, 238 (1963).
[62] A. Östlin, L. Vitos, and L. Chioncel, Phys. Rev. B **98**, 235135 (2018).
[63] H. Shiba, Prog. Theor. Phys. **46**, 77 (1971).
[64] N. J. Higham, *Accuracy and Stability of Numerical Algorithms*, Other Titles in Applied Mathematics (Society for Industrial and Applied Mathematics, Philadelphia, 2002).
[65] E. H. Moore, Bull. Am. Math. Soc. **26**, 454 (1920).
[66] R. Penrose, Math. Proc. Cambridge Philos. Soc. **51**, 406 (1955).